AEROELASTIC ANALYSIS OF A JOINED-WING SENSORCRAFT

THESIS

Jennifer J. Sitz, Lieutenant, USAF

AFIT/GAE/ENY/04-J12

DEPARTMENT OF THE AIR FORCE
AIR UNIVERSITY

AIR FORCE INSTITUTE OF TECHNOLOGY

Wright-Patterson Air Force Base, Ohio

AFIT/GAE/ENY/04-J12

AEROELASTIC ANALYSIS OF A JOINED-WING SENSORCRAFT

THESIS

Presented to the Faculty
Department of Aeronautical and Astronautical Engineering
Graduate School of Engineering and Management
Air Force Institute of Technology
Air University
Air Education and Training Command
In Partial Fulfillment of the Requirements for the
Degree of Master of Science in Aeronautical Engineering

Jennifer J. Sitz, BS
1Lt, USAF

June 2004

AFIT/GAE/ENY/04-J12

Aeroelastic Analysis of a Joined-Wing SensorCraft

Jennifer J. Sitz, BS
1Lt, USAF

Approved:

Lt Col Robert Canfield (Chairman)	date
Lt Col Montgomery Hughson (Member)	date
Dr. Don Kunz (Member)	date

Acknowledgements

I would like express my sincere gratitude to my thesis advisor, Lt Col Robert A. Canfield, for his guidance, support, and patience throughout this effort. I would also like to thank Dr. Maxwell Blair of the Air Force Research Laboratory for his software support and guidance, Capt Ronald Roberts and Capt Cody Rasmussen, on whose work this effort is based, and Christopher Buckreus for his indispensable assistance. Finally, I would like to thank my boss, Dr. William Borger, and Col Donald Huckle for their support of this effort.

Special thanks go out to my husband for his patience, unyielding support, and love.

Jennifer J. Sitz

Table of Contents

List of Figures

List of Tables

Abstract

This study performed an aeroelastic analysis of a joined-wing SensorCraft. The analysis was completed using an aluminum structural model that was splined to an aerodynamic panel model. The force and pressure distributions were examined for the four aerodynamic panels: aft wing, fore wing, joint, and outboard tip. Both distributions provide the expected results (elliptical distribution), with the exception of the fore wing. The fore wing appears to be affected by interference with the joint. The use of control surfaces for lift and roll was analyzed. Control surfaces were effective throughout most of the flight profile, but may not be usable due to radar requirements. The aft wing was examined for use in trimming the vehicle. Also, two gust conditions were examined. In one model, the wing twist was simulated using a series of scheduled control surfaces. Trim results (angle of attack and twist angle) were compared to those of previous studies, including gust conditions. The results are relatively consistent with those calculated in previous studies, with variations due to differences in the aerodynamic modeling. To examine a more physically accurate representation of aft wing twist, it was also modeled by twisting the wing at the root. The twist was then carried through the aft wing by the structure. Trim results were again compared to previous studies. While consistent for angle of attack results, the aft wing twist deflection remained relatively constant throughout the flight profile and requires further study.

AEROELASTIC ANALYSIS OF A JOINED-WING SENSORCRAFT

I. Introduction

Overview

Recent events such as Operation Iraqi Freedom and the conflict in Afghanistan have shown an increased interest in the use of unmanned aerial vehicles (UAVs), particularly as surveillance-type platforms. UAVs seem especially suited for intelligence/surveillance/reconnaissance (ISR) missions, which require many hours of continuous coverage at high altitudes. One ISR concept, known as SensorCraft, includes missions such as targeting, tracking, and foliage penetration (tanks under trees). Several of these missions require large antennas, and some demand 360 degree coverage. All of these requirements, but especially the endurance, demand the use of a UAV. Several configurations are currently being considered for the SensorCraft mission. A conventional vehicle, similar to Global Hawk, is a possibility. However, Global Hawk or a similar conventional configuration cannot provide 360-degree continuous coverage of the area of interest. Another possibility is a flying wing body, with sensors conformally integrated into the highly swept wings. For this effort, however, another configuration is studied, the joined-wing. Such a design lends itself to continuous 360-degree coverage, while possibly providing weight savings and improved aerodynamic performance over a conventional vehicle. The joined-wing typically consists of a large lifting surfacing, the

aft wing, which connects to the top of the vertical tail and sweeps forward and down to connect to the main, or fore, wing of the vehicle (Figures 1-1, 1-2).

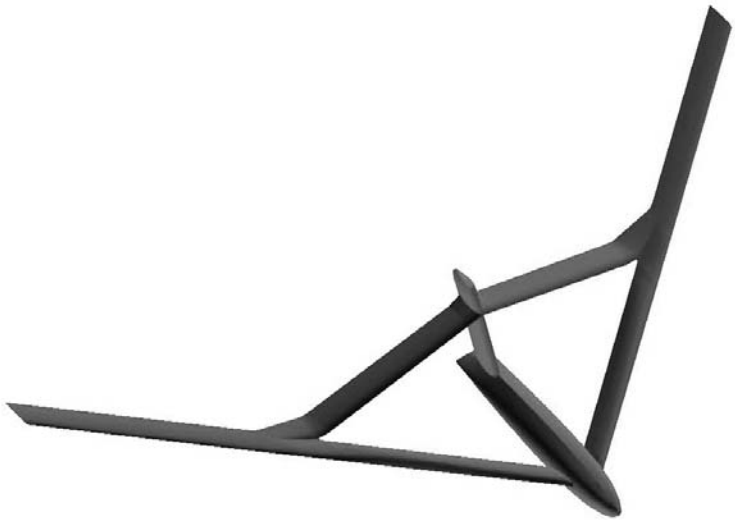

Figure 1-1: Sample Total Joined Wing Configuration Concept

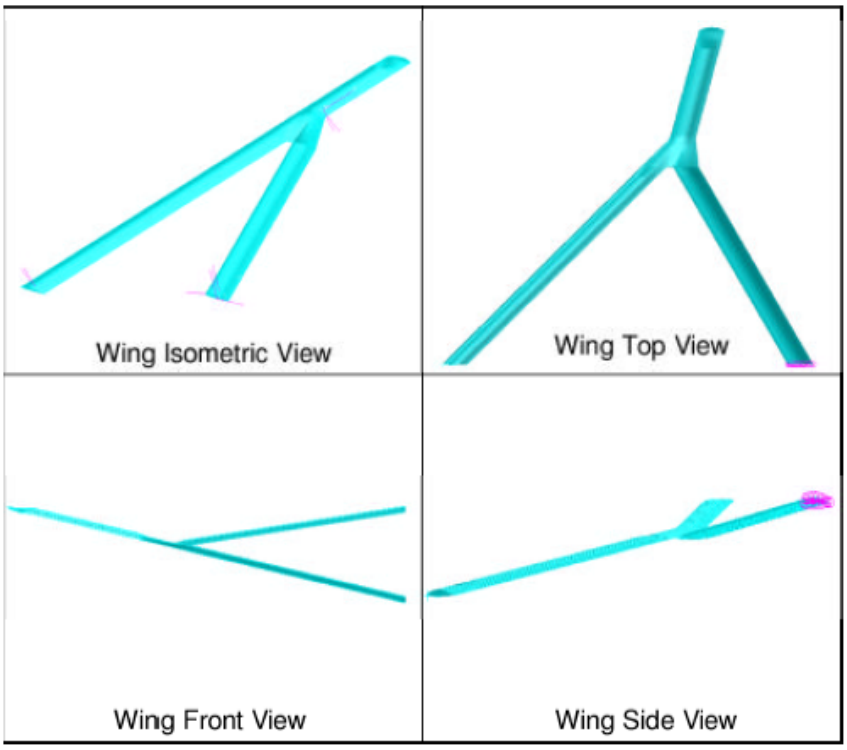

Figure 1-2: Various Joined-Wing Viewing Angles

To accommodate all the demands of a joined-wing SensorCraft, it is crucial that the design process examine the aerodynamic, structural and payload influences simultaneously. For example, flexible aeroelastic loads are needed to provide realistic estimates of aerodynamic performance, and conformal antennae provide a significant portion of the load-bearing structure. While the efforts of this paper concentrate on the aerodynamic performance and efficiency of the joined-wing, they are fundamentally tied to previous and concurrent efforts examining the sensors and structure of such a vehicle.

The proposed SensorCraft design uses conformal radar antennae in the fore and aft wings to provide 360 degree UHF surveillance of the area of interest and structural support to the vehicle. UHF is the radar frequency required for foliage penetration (FOPEN), allowing radar to image a target beneath a canopy of vegetation. The Conformal Load-bearing Antenna Structure (CLAS) is built into the wing structure, and is a composite sandwich of Graphite Epoxy, Carbon foam core, and an Astroquartz skin covering (Figure 1-3). Antenna elements are attached to the graphite/epoxy layers, and the Astroquartz provides environmental protection and an electro-magnetically clear material for the radar to transmit through.

Figure 1-3: Conformal Load-bearing Antenna Structure Cross Section

The proposed SensorCraft span is 66 meters, or approximately 200 ft, which would result in large bending moments in the front wing. The aft wing, therefore, is used as a support strut to minimize those moments. As a result, the aft wing undergoes axial compression, potentially causing the wing to buckle, and the fore wing does still experience bending moments and thus large deflections. The method used to structurally analyze these large deflections is a non-linear finite element analysis.

Research Objectives

This research examined the effectiveness of conventional control surfaces for roll and lift on a joined-wing, focusing on where control surfaces should be located to avoid reversal. This research used the double lattice subsonic lifting surface theory of MSC.Nastran to trim the joined-wing for flexible loads, and compared those results to the results developed by Roberts using PanAir [1]. For the trim studies, aft wing twist was used for vehicle control via a series of scheduled control surfaces.

Research Focus

This research focused on the aerostructural analysis of a joined-wing SensorCraft. The panel method of MSC.Nastran was used to examine the use of control surfaces and validate the aerodynamic trim calculated in previous efforts that concentrated on optimizing the vehicle for minimal weight.

Methodology Overview

The weight-optimized, aluminum structural model from the work of Roberts [1] was used as the basis for this effort. That research used Adaptive Modeling Language (AML) to develop a geometric model that contains all the necessary information to perform multi-disciplinary analysis. The Air Vehicle Technology Integration

Environment (AVTIE), developed by Dr. Max Blair, allows the user to develop the aerodynamic and structural models from the AML geometric model [19]. AVTIE also performs the aerodynamic trim calculations. The AVTIE structural model and aerodynamic trim calculations developed by Roberts were used as the baseline for this effort.

The structural model was imported into MSC.FlightLoads where the aerodynamic model was created and splined to the structural model. Two conditions were examined – the first used conventional control surfaces for lift and roll, the second used the twist of the aft wing to trim for 1.0G cruise and 2.5G maneuvers. Once the aerodynamic model was developed, MSC.Nastran was used to examine the control surface effectiveness of conventional surfaces and the trim results of twisting the aft wing for aerodynamic control. To compare trim results to those of Roberts [1], aft wing twist was modeled using scheduled control surfaces. The aircraft was trimmed for angle of attack and twist angle for a 2.5G maneuver.

Assumptions and Limitations

The structural model used in this study is the aluminum model by Roberts [1]. For his work, we assume the structure is made of linear materials and experiences linear deformations. The PanAir aerodynamic analysis utilizes an inviscid panel method. Fixed L/D was assumed in calculating the fuel consumed.

This study took the previously mentioned structural model, created a corresponding flat panel aerodynamic model, and splined the two models together. The aerodynamic model was created by defining four panels, each of which was divided into 100 boxes (ten chordwise and ten spanwise). This mesh was assumed to be sufficient to

provide relevant results. To take camber into account, a matrix of aerodynamic box slopes was manually entered into the model. Finally, four splines were created by connecting the four aerodynamic panels to the structural model at three chordwise and twenty-one spanwise locations for the fore and aft wings, four chordwise and eleven spanwise locations for the joint, and four chordwise and seventeen spanwise locations for the outboard tip.

Aft wing twist was modeled using a series of ten scheduled control surfaces along the aft wing. The surfaces were scheduled such that the most inboard panel was free to twist to trim the vehicle. Each consecutive surface was than linked to the one before at 10% of the previous deflection. This setup assumes a linearly tapered aft wing twist, which may not be true in reality due to uneven structural composition. It can also cause inconsistencies due to gaps between the deflected control surfaces.

Implications

This study validates and expands on the aerostructural analysis of previous efforts. MSC.Nastran allows a researcher to examine the effects of control surfaces, aft wing twist, and aeroelastic trim. This research demonstrated that a joined wing configuration can support the demanding SensorCraft requirements.

II. Literature Review

Past Joined-Wing Design Efforts

Beginning in 1976 when Wolkovitch [2] first patented his joined-wing concept, this particular configuration has been studied by a number of designers hoping to capitalize on the structural and aerodynamic advantages the joined-wing appears to offer. In 1985, Wolkovitch [3] published an overview of his joined-wing concept based on wind tunnel analysis and finite element structural analysis. The study claimed that the joined wing provides several advantages over a conventional configuration, including light weight, high stiffness, low induced drag, high trimmed C_L max, and good stability and control, among other advantages.

Early in the study of joined-wing concepts, Fairchild performed a structural weight comparison between a joined wing and a conventional wing [4]. Using a NACA 23012 for both wings, he held the thickness ratio and structural box size constant throughout the study. An examination of the joined-wing skin thickness distribution showed it differed from the conventional configuration in that there was: a) the evidence of two distinct maxima on each wing surface, and b) a different chordwise taper on the upper and lower skins. Another difference shows a 50% reduction of joined-wing vertical deflection over the conventional configuration. This is obviously an advantage, but the study also found a noticeable difference in the deflections of the fore and aft wings of the joined-wing. Fairchild suggested that this is caused by a combination of tension and compression in each wing, or twist, and identifies it as a point for further

study. Finally, the study finds that for aerodynamically equal configurations, the joined-wing was approximately 88% of the conventional configuration weight.

Shortly after Wolkovitch published his review of the joined-wing, Smith et al. studied the design of a joined-wing flight demonstrator aircraft [5]. The effort designed the demonstrator based on the existing NASA AD-1 flight demonstrator aircraft, and performed a wind tunnel test in the NASA Ames 12-foot wind tunnel. In this case, the joined-wing was examined for use as a transport aircraft flying at Mach 0.80 at its best cruising altitude. The study found that the optimum interwing joint location was at 60% of the fore wing semispan. Using vortex-lattice methods, the wing incidence distribution was designed, and NACA 6-series airfoils were used to optimize the lift coefficient. Finally, good stall characteristics were seen as essential, even to the detriment of cruise performance. The related wind tunnel tests showed good agreement with the design predictions in the areas of performance, stability and control.

A design study of joined-wings as transports was performed by Gallman et al. [6]. This study examined aerodynamics and structure, but also looked at the potential direct operating cost (DOC) savings for the joined wing as compared to a conventional configuration. A joined-wing with a joint location at 70% of the wing semispan was examined, and a 2000 nm transport mission was considered. Under these assumptions, it was found that an optimized joined-wing will provide a 1.7% savings in direct operating cost and an 11% savings in drag over a conventional DC-9-30 aircraft. However, if examined at off-design points such as takeoff, the savings in DOC decreases by about 1%. Another key lesson learned was the increase required in wing area or engine size

due to tail downloads, an indication of the importance of considering the maximum lift capability.

Wai et al. performed a computational analysis of a joined-wing configuration using a variety of methods and solvers [7]. The numerical results using unstructured Euler and structured Navier-Stokes flow solvers were compared to experimental results based on a 1/10 model tested in the NASA LaRC 16 foot transonic tunnel. The numerical results indicate that the stagnation condition at the joint causes a severe adverse pressure gradient. This causes boundary layer separation to spread spanwise onto the wing tip and inboard section. Overall, the viscous results agree with the experimental data in terms of both surface pressures and flow orientation, proving that numerical computations provide useful design information.

Another computational analysis was performed by Tyler et al., in order to better understand the aerodynamics of the joined-wing [8]. To validate the CFD computations performed using $Cobalt_{60}$, a wind tunnel test was also completed in the Langley Basic Aerodynamics Research Tunnel. The computational grid was designed to model the wind tunnel walls and sting, as well as the configuration, in order to better relate the results. The test found that there is more interaction between the fore and aft wings at higher angles of attack, and separation becomes noticeable at an angle of attack of -5 degrees.

Joined-Wing Survey

Livne [9] provided a valuable survey of developments in the design of joined-wing configurations. He identified the need for collaboration between different technological disciplines, and summarized the benefits and limitations learned in past

aeroelastic studies of joined-wings. Specifically, Livne noted that in previous studies in-plane compressive loads in the aft tail were not always considered, that the sensitivity of flutter relates to fuselage stiffness, and that tail divergence is a critical aeroelastic instability. He goes on to note that the aircraft can be designed to prevent buckling, but that efforts to minimize weight may negatively affect this area of structural optimization, as well as many others.

Several other authors examined the structure and aeroelasticity of the joined-wing configuration. Gallman and Kroo identified the differences between fully stressed and minimum-weight joined-wing structures [10]. They found the fully stressed structure is a good approximation, and that for the transport mission the joined-wing is slightly more expensive than a conventional configuration when aft wing buckling is considered. Reich et al. examined the feasibility of using the active aeroelastic wing (AAW) technology on a joined-wing SensorCraft in order to minimize embedded antenna deformations [11].

Basis for Current Research

Configuration Design Tools

Several configuration design tools are used in this study. The Adaptive Modeling Language (AML) tool [12] was developed by TechnoSoft and uses geometric objects to produce a full wing-body. This can then be input into PanAir, a linear aerodynamic solver that implements a higher order panel method [13]. MSC.FlightLoads [14] is another panel method, but has several advantages over PanAir. Specifically, it can be used to trim the vehicle in question, in addition to calculating flight loads. It also links

the aerodynamics and flight load calculations to MSC.Nastran, a finite element program. This is a vital role in the design of a joined-wing [14, 15, 16].

Recent Work

The current study began with the efforts of Blair et al. to develop advanced design tools and processes suitable for the design of a joined-wing aircraft, specifically SensorCraft [17]. In order to address the factors of cost estimation, structural finite element modeling, optimization, computational fluid dynamics, and control system synthesis, they developed a design process that integrates aerodynamics and structural loads. The process begins with the development of Adaptive Modeling Language (AML) objects, which can be used to "build" a blended surface for panel definitions to drive PanAir input, CFD calculations, and a structural finite element modeler. Drag calculations made with the linear aerodynamic solver PanAir [13] can be compared to those from CFD [18], and the structural results of the finite element modeler can be used to update the aerodynamic mesh. This interactive design capability is essential to the design process for a joined-wing.

In a follow-on to the work done by Blair et al., Blair and Canfield provide further definition for the current study in their structural weight modeling study of a joined-wing [19]. In this study, an integrated, iterative design process was used to develop high-fidelity weight estimations of joined-wings. Specifically examined were the non-linear phenomena identified as large deformation aerodynamics and geometric nonlinear structures. Important results include recognition of the need for examining the nonlinear response in the design and performing a complete model for drag estimation, including all effects.

The majority of this effort is based on the Master's work of Roberts [16] and Rasmussen [17]. Roberts performed a multi-disciplinary conceptual design of a joined-wing SensorCraft, and showed that there is a strong aerodynamic and structural coupling. Specifically, changes in deformation, weight, fuel required, angle of attack, aft-wing twist angle, or payload location can all affect the aerodynamic and structural characteristics of the vehicle. The study optimized the design structurally and examined the impact of the results on the aerodynamics. Rasmussen established a weight optimized configuration design of a joined-wing SensorCraft by examining 74 configurations that varied one of the following geometric variables: fore wing sweep, aft wing sweep, outboard tip sweep, joint location, vertical offset, and thickness to chord ratio. His results showed that a designer may trade vertical offset against thickness to chord ratio or fore wing sweep against aft wing sweep.

III. Methodology

Previous Work

The SensorCraft mission places an unusual and extensive set of demands that drives the need to use the joined-wing configuration. The driving objectives are listed below:

- 3,000 nm radius
- 24 hours time on station (TOS)
- Loiter at 55,000 – 65,000 ft altitude
- 4,880 lb payload (baseline)
- <200 ft span (for basing purposes)
- 360-degree radar coverage over a wide area utilizing both high and low band antenna

These objectives must be achieved throughout the design mission. For the purpose of this study, the Global Hawk mission profile will be used, as listed below and shown in Figure 3-1.

1. Takeoff
2. Climb to 50,000 ft altitude for 200 nm
3. Cruise from 50,000 ft for 3000 nm ingress
4. Loiter at 65,000 ft for 24 hours
5. Cruise from 50,000 ft for 3000 nm egress
6. Descend to zero ft altitude for 200 nm
7. Land at zero ft altitude

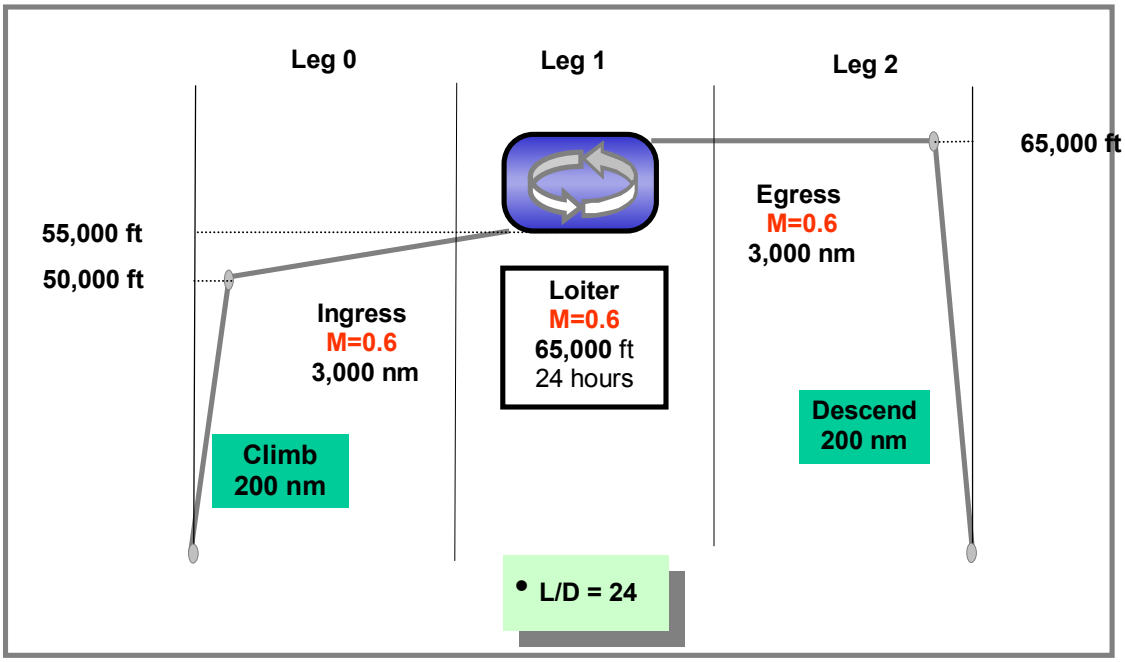

Figure 3-1: Notional Mission Profile

As a baseline, we assume an L/D of 24 is achievable at Mach 0.6 for ingress, loiter, and egress. Assume also that the coefficient of brake horsepower, C_{bhp}, is 0.55 and the propeller efficiency is assumed to be 0.8. The baseline aerodynamic parameters are shown in Table 3-1.

Table 3-1: Baseline Aerodynamic Parameters

	Ingress (0)	Loiter (1)	Egress (2)
Range	3000 nm 5550 km	N/A	3000 nm 5550 km
Duration	N/A	24 hr 8.64E4 s	N/A
Velocity	0.6 Mach @ 50k ft 177 m/s	0.6 Mach @ 65k ft 177 m/s	0.6 Mach @ 50k ft 177 m/s
C (SFC)	2.02E-4 (1/sec)	1.34E-04 (1/sec)	2.02E-4 (1/sec)
Dynamic Pressure	2599 Pa	1269 Pa	2599 Pa
Wa/Wb	1.32	1.62	1.33

To achieve the performance goals above, a joined-wing configuration is examined at various points throughout the mission. Figure 3-2 displays the geometric design of the vehicle with configuration parameters identified, and Table 3-2 specifies the baseline parameter values.

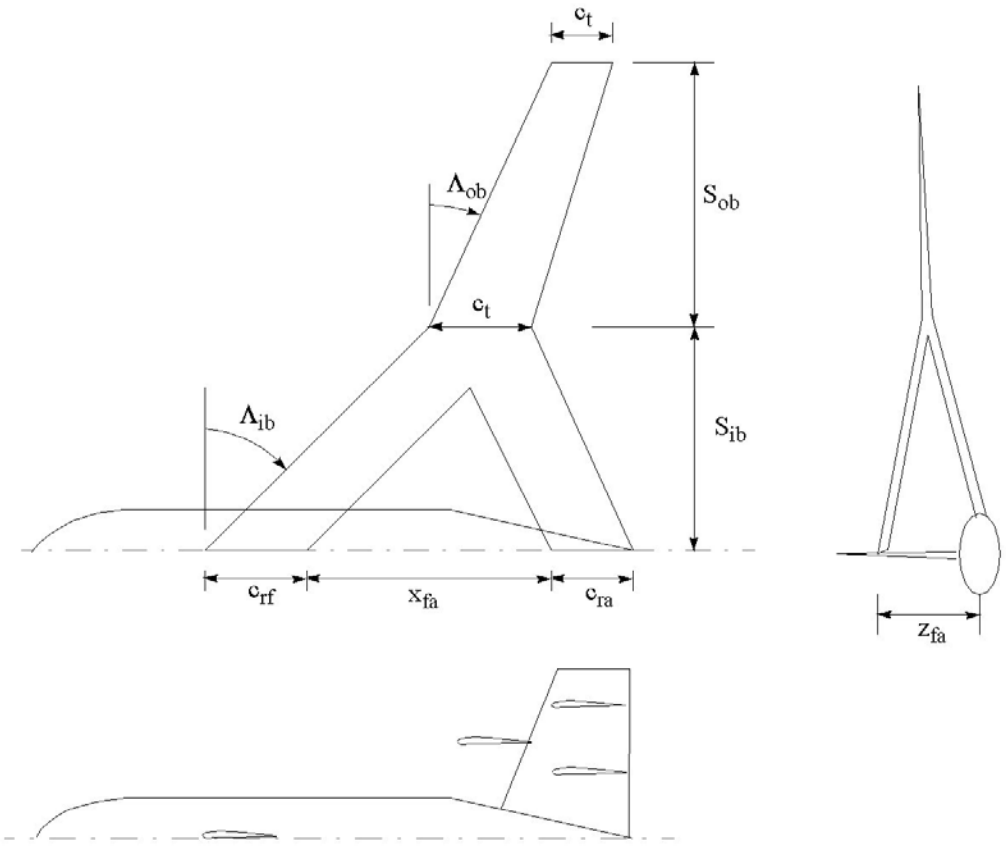

Figure 3-2: Planform Configuration

Table 3-2. Baseline Configuration Parameters

Inboard Span	S_{ib}	26.00 m
Outboard Span	S_{ob}	6.25 m
Forward Root Chord	c_{rf}	2.50 m
Aft Root Chord	c_{ra}	2.50 m
Mid Chord	c_m	2.50 m
Tip Chord	c_t	2.50 m
Forward-aft x-offset	x_{fa}	22.00 m
Forward-aft z-offset	z_{fa}	7.00 m
Inboard Sweep	Λ_{ib}	30 deg
Outboard Sweep	Λ_{ob}	30 deg
Airfoil		LRN-1015
Calculated Planform Area		145.0 m^2
Calculated Wing Volume		52.2 m^2

AVTIE Model and Environment

Previous studies by Roberts and Rasmussen used the Air Vehicles Technology Integration Environment (AVITE), which was developed by Blair and Canfield [19], to interface with the Adaptive Modeling Language (AML) program. AML was developed by TechnoSoft, Inc., and allows the user to develop a geometric model using mathematical relationships. AVTIE builds a geometric surface model from configuration data, then converts the geometric model into data files for analysis with external software such as MSC.Nastran. AVTIE also interprets the output data from these programs and updates the geometric model as required.

For these efforts, AVTIE uses the mission profile information previously highlighted in Table 3-1. The mission is divided into segments known as ingress (leg 0), loiter (leg 1), and egress (leg 2). These segments are then subdivided, resulting in mission points at the beginning and middle of ingress (0-00 and 0-50), beginning and middle of loiter (1-00 and 1-50), and beginning, middle, and end of egress (2-00, 2-50, and 2-98) as shown in Table 3-3. The first digit in the number indicates the mission leg,

and the last two digits represent the percentage of that leg completed. The multiple points per mission segment are necessary because the weight reduction due to burnt fuel changes the trim angles and therefore the load distribution. The performance information is used to provide the weight of the remaining fuel at any point in the mission.

Table 3-3: Mission Load Sets

Mission Load Number	Load Type	Mission Category	Category Complete
0-00	Maneuver	Ingress	0%
0-50	Maneuver	Ingress	50%
1-00	Maneuver	Loiter	0%
1-50	Maneuver	Loiter	50%
2-00	Maneuver	Egress	0%
2-50	Maneuver	Egress	50%
2-98	Maneuver	Egress	98%
2-98c	Cruise Gust	Egress	98%
2-98t	Turbulent Gust	Egress	98%

Gust Loading

To fully analyze the aircraft for all situations, the gust condition must be considered. In this study, the aircraft is flying straight and level at 1.0G, so the lift load equals the aircraft weight. The vehicle then experiences an instantaneous vertical gust wind of velocity U_g that rapidly changes the angle of attack, as shown in Figure 3-3.

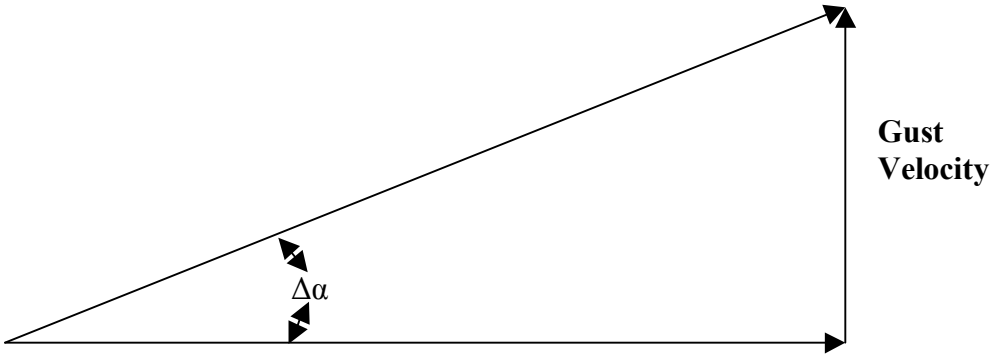

Figure 3-3: Gust Velocity Component

The increase in angle of attack also results in an increase in lift, as shown in Equations 3-1 and 3-2. As fuel is burned and the weight of the aircraft decreases, the load factor increases. Therefore, a gust at the end of the mission will cause the highest load factor increase.

$$\Delta\alpha = \frac{U_g}{V} \tag{3-1}$$

$$\Delta L = \frac{1}{2} C_{l_\alpha} \Delta\alpha \rho V^2 S \tag{3-2}$$

The previous equations assume an instantaneous gust load, but throughout an actual mission an aircraft will generally fly into a gust condition, which can reduce the load factor. This is the gust alleviation factor K which can be defined using the airplane mass ratio μ_g as shown in Equations 3-3 and 3-4.

$$K = \frac{0.88\mu_g}{5.3 + \mu_g} \tag{3-3}$$

$$\mu_g = \frac{2W}{S\rho C_{l_\alpha} cg} \tag{3-4}$$

Roberts examined a cruise gust condition and a turbulent gust condition [1]. For the cruise condition, the gust velocity is 50 ft/s, while the gust velocity for the turbulent condition is 66 ft/s. The gust velocities occur in both the positive and negative directions, and are used up to 20,000 ft. Roberts determined that the critical gust case is the turbulent gust situation where the vertical gust velocity is the largest.

PanAir Aerodynamic Analysis

PanAir analyzes an aerodynamic model consisting of panel elements. A blended surface was created in AVTIE to be used as an IGES file for panel definitions to drive PanAir and MSC.FlightLoads input. Figure 3-4 shows the baseline PanAir panel configuration that AVTIE generates. AVTIE provides PanAir with dynamic pressure information based on the mission point to be analyzed and transfers angle of attack and aft-wing twist information. PanAir calculates interpolated pressures at the panel corners, which AVTIE then integrates and distributes over the structural model's fore and aft wings. AVTIE provides aerodynamic center and center of pressure information, total lift force, and induced drag forces [1].

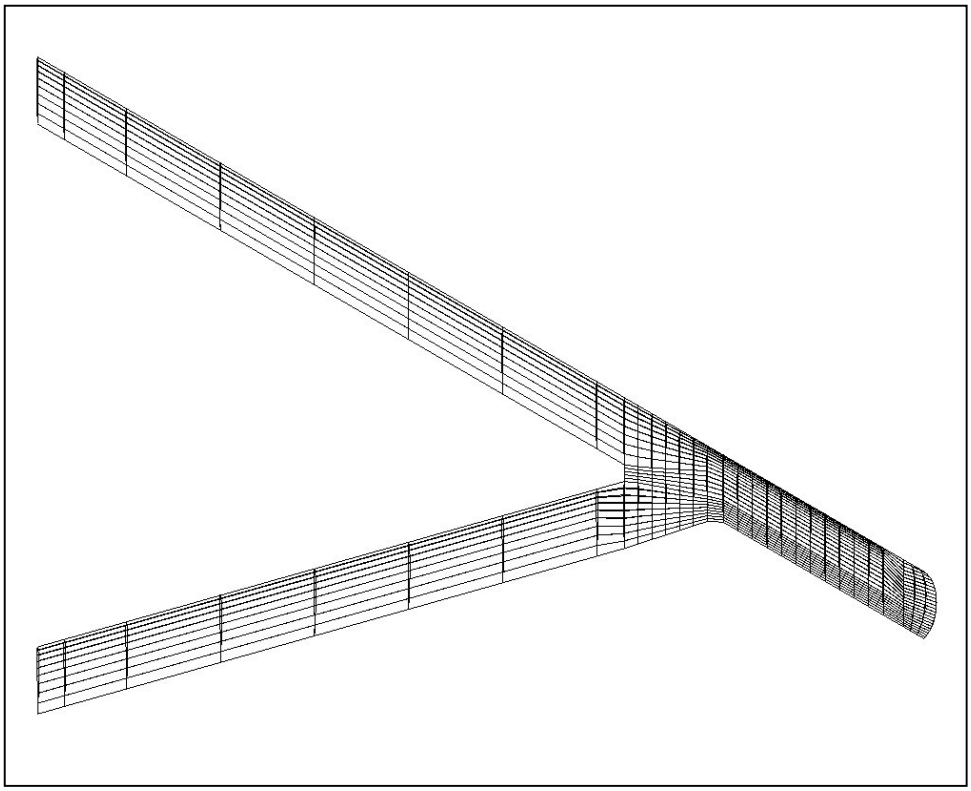

Figure 3-4: PanAir Baseline Geometry with 30 Degrees Sweep (Plan View)

PanAir Trim for Rigid Aerodynamic Loads

In the work of Roberts, lift and pitch trim is controlled by the aircraft angle of attack and aft-wing flexible twist angle. The aft wing is rotated at the root and is fixed at the joint, while an unmodeled actuator in the vertical tail drives the twist angle. Trim in AVTIE is based on a series of linear Taylor series approximations based on the angle of attack α and the aft-wing-root-twist, δ as shown in Equation (3-5). PanAir is then used to regenerate the pressure distributions at the trimmed conditions.

$$\begin{Bmatrix} C_L - C_{L0} \\ C_M - C_{M0} \end{Bmatrix} = \begin{bmatrix} \left(\frac{dC_L}{d\alpha}\right) & \left(\frac{dC_L}{d\delta}\right) \\ \left(\frac{dC_M}{d\alpha}\right) & \left(\frac{dC_M}{d\delta}\right) \end{bmatrix} \begin{Bmatrix} \alpha - \alpha_1 \\ \delta - \delta_1 \end{Bmatrix} \tag{3-5}$$

PanAir trims the aircraft for a steady, pull-up or turn maneuver at a 2.5G load at the previously mentioned mission points by relocating the payload mass to adjust the center of gravity. Static stability requires that the center of gravity be forward of the aerodynamic center, and pitch trim requires that the center of gravity be at the center of pressure. The payload location required for static stability is calculated in Equation (3-6). Once the payload mass is moved to the appropriate location, it is fixed for the entire mission.

$$\left|X_{cg} - X_{ac}\right| \cdot \frac{TotalMass}{PayloadMass} = \Delta X_{cg} \tag{3-6}$$

PanAir Trim for Flexible Aerodynamic Loads

After trimming for rigid loads, AVTIE recalculates X_{cg} and the fuel required to complete the mission. The PanAir model is then updated to account for flexible deformation, and PanAir generates new aerodynamic loads based on the deformed model. Using Equation (3-5), AVTIE retrims the aircraft, and then payload mass balancing may be used again if center of gravity changes demand it.

Current Study

Doublet-Lattice Subsonic Lifting Surface Theory

The structural models used in this study were developed by Roberts, Canfield, and Blair in a concurrent study [20]. In the current effort, MSC.Patran was utilized to develop the load and boundary conditions; the results were then loaded into MSC.FlightLoads. MSC.FlightLoads creates aerodynamic models and produces results that are compatible with the Doublet-Lattice aerodynamics that are provided in

MSC.Nastran. The Double Lattice method (DLM) applies to subsonic flows and is a panel method that represents lifting surfaces by flat panels that are nominally parallel to the flow. MSC.Nastran aerodynamic analysis is based upon a boundary element approach, where the elements are boxes in regular arrays with sides that are parallel to the airflow. Aerodynamic forces are generated when the flow is disturbed by the flexible vehicle. These deflections are the combination of rigid body motions of the vehicle and the structural deformations of the vehicle as it undergoes applied loading during a maneuver. For the steady flow considered in the static aeroelastic analysis, the relationship between the deflection and the forces is a function of the aerodynamic model and the Mach number of the flow.

The aerodynamic grid points for DLM are located at the centers of the lifting surface elements, with another set of grid points, used for display, located at the element corners. Grid point numbers are generated based upon the panel identification number. The grids for the centers of the aerodynamic boxes are numbered from the inboard leading edge box and then incremented by one, first in the chordwise direction and then spanwise. The corner grid numbering begins at the leading edge inboard corner and also proceeds chordwise then spanwise. The flat plate aerodynamic methods solve for the pressures at a discrete set of points contained within these boxes. Doublets are assumed to be concentrated uniformly across the one-quarter chord line of each box. There is one control point per box, centered spanwise on the three-quarter chord line of the box, and the surface normalwash boundary condition is satisfied at each of these points. The doublet magnitudes are determined so as to satisfy the normalwash condition at the control points.

The aerodynamic theory used in this study, Doublet-Lattice subsonic lifting surface theory, can be used for interfering lifting surfaces in a subsonic flow. It consists of a matrix structure that uses three equations to summarize the relationships required to define a set of aerodynamic influence coefficients. These are the basic relationships between the lifting pressure and the dimensionless vertical or normal velocity induced by the inclination of the surface to the airstream, Equation (3-7), the substantial differentiation matrix of the deflections to obtain downwash, Equation (3-8), and the integration of the pressure to obtain forces and moments, Equation (3-9).

$$\{w_j\} = [A_{jj}]\left\{\frac{f_j}{\bar{q}}\right\} \tag{3-7}$$

$$\{w_j\} = [D_{jk}]\{u_k\} + [D_{jx}]\{u_x\} + \{w_j^g\} \tag{3-8}$$

$$\{P_k\} = [S_{kj}]\{f_j\} \tag{3-9}$$

where:

w_j = downwash

w_j^g = static aerodynamic downwash, it includes, primarily, the static incidence distribution that may arise from an initial angle of attack, camber, or twist

f_j = pressure on lifting element j

$\overline{q}$ = flight dynamic pressure

$A_{jj}(m)$ = aerodynamic influence coefficient matrix, a function of Mach number (m)

u_k = displacements at aerodynamic grid points

P_k = forces at aerodynamic grid points

D_{jk} = Substantial differentiation matrix for aerodynamic grid deflection (dimensionless)

$[D_{jx}]$ = substantial derivative matrix for the extra aerodynamic points

$\{u_x\}$ = vector of "extra aerodynamic points" used to describe, e.g., aerodynamic control surface deflections and overall rigid body motions

S_{kj} = integration matrix

The three matrices of Equations (3-7), (3-8), and (3-9) can be combined to give an aerodynamic influence coefficient matrix, Equation (3-10), with relates the force at an aerodynamic grid point to the deflection at that grid point and a rigid load matrix, Equation (3-11) which provides the force at an aerodynamic grid point due the motion of an aerodynamic extra point.

$$[Q_{kk}] = [S_{jk}][A_{jj}^{-1}][D_{jk}] \tag{3-10}$$

$$[Q_{kx}] = [S_{kj}][A_{jj}^{-1}][D_{jx}] \tag{3-11}$$

The theoretical basis of DLM is linearized aerodynamic potential theory. All lifting surfaces are assumed to lie nearly parallel to the flow, which is uniform and either steady or gusting harmonically. The A_{jj}, S_{kj}, and D_{jk} matrices are computed as a function of Mach number, with the D_{jk} matrix calculated only once since it is a function only of the model geometry. Any number of surfaces can be analyzed, and aerodynamic symmetry options are available for motions which are symmetric or antisymmetric with respect to one or two orthogonal planes, as long as the user imposes the appropriate structural boundary conditions.

Two Dimensional Finite Surface Spline

To be analyzed as an aerostructural model, the aerodynamic model must then be coupled to the structural model using a two dimensional finite surface spline. In the context of MSC.FlightLoads, splines provide an interpolation capability that couples the disjoint structural and aerodynamic models in order to enable the static aeroelastic analysis. They are used for two distinct purposes: as a force interpolator to compute a structurally equivalent force distribution on the structure given a force distribution on the aerodynamic mesh and as a displacement interpolator to compute a set of aerodynamic displacements given a set of structural displacements. The force interpolation is represented mathematically in Equation (3-11) and the displacement interpolation in Equation (3-12) as:

$$[F_s] = [G_{sa}][F_a] \tag{3-11}$$

$$[U_a] = [G_{as}][U_s] \tag{3-12}$$

where G is the spline matrix, F and U refer to forces and displacements, respectively, and the s and a subscripts refer to structure and aerodynamics, respectively. The finite surface spline is a method that uses a mesh of elemental quadrilateral or triangular plates to compute the interpolation function. The interpolent is based on structural behavior, and the equations are a discretized approximation of a finite structural component [15].

In this study, four lifting surfaces that match the structural model were created by specifying the structural grid points of the fore wing, aft wing, joint, and outboard wing tip. Each surface was then meshed with ten uniform aerodynamic panels in both the chord- and spanwise directions, as demonstrated in Figure 3-5. The splines were connected to grid points on the substructure (Figure 3-3) so that the integrated forces were properly transferred through the stiffer points in the wing box. As shown in Figure 3-6, the splines were connected to the upper surface of the wing. The wing box will then transfer the forces through the wing box via the spars and ribs.

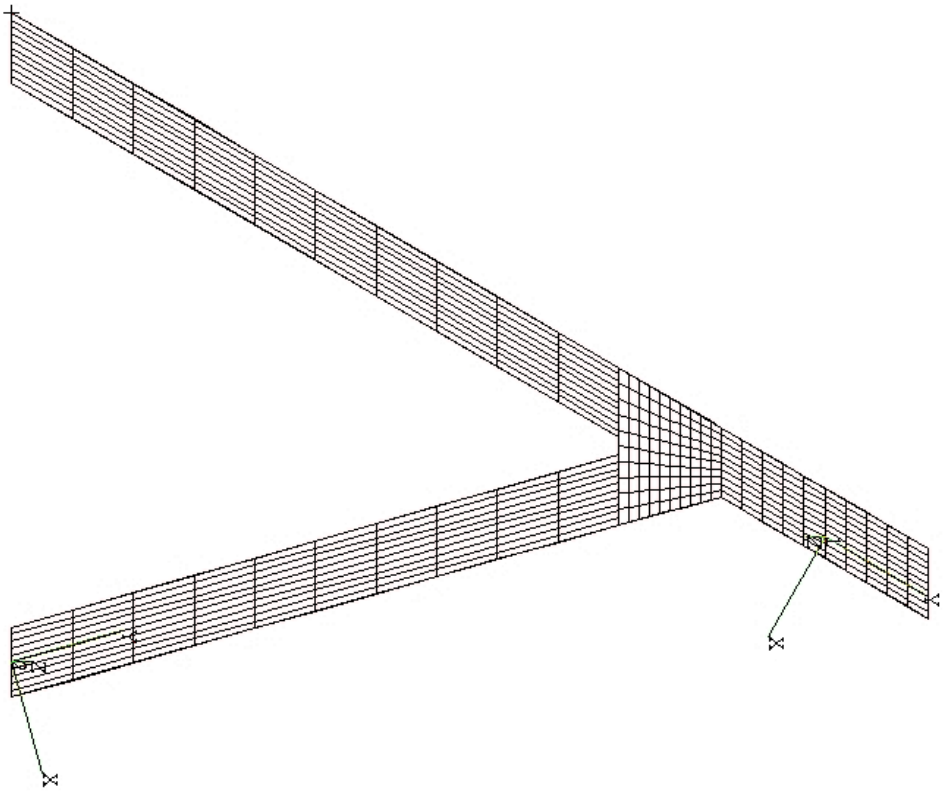

Figure 3-5: Joined-Wing Lifting Surface Mesh

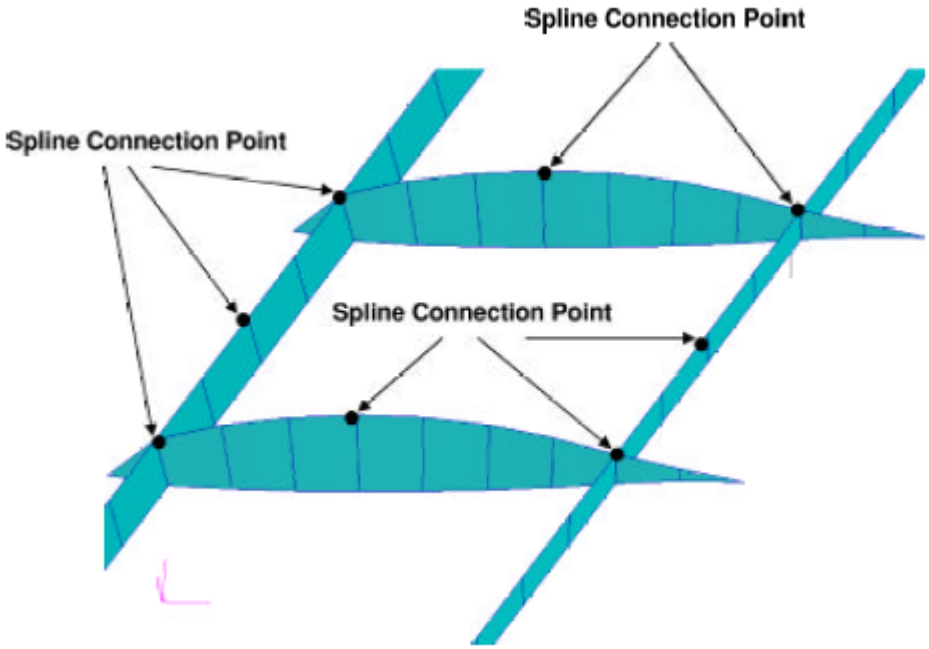

Figure 3-6: Spline Locations

Camber Modeling

The surface fitted PanAir model developed by Roberts includes the camber of the airfoil, but MSC.Flightloads models the aerodynamics using flat plates. To include the camber in the MSC.Nastran analysis, it must be modeled by manually inputting the camber slopes of each box's control point. Specifically, the streamwise camber slope of each box is used to adjust satisfaction of the no penetration boundary conditions at each collocation point. In this case, the matrix being input is a real, single precision rectangular matrix known as a W2GJ matrix. This is the $\{w_j^g\}$, or camber, term of Equation (3-8), where the values are derived by the user at the aerodynamic grid points of all aerodynamic boxes and slender body elements. This is done by defining direct input matrices related to collocation degrees of freedom of aerodynamic mesh points, or DMIJ cards. The matrix is defined by a header entry that names the matrix, describes the form and type of the matrix being input, and the type of matrix being created [16]. The output matrix type is set by the precision system cell. The actual matrix input values are then entered using a column entry format which specifies the aerodynamic box and the real part of the matrix element (the amplitude). The bulk data for the camber modeling can be found in Appendix A.

Static Aeroelasticity Analysis

Static aeroelastic problems deal with the interaction of aerodynamic and structural forces on a flexible vehicle. This interaction causes a redistribution of aerodynamic loading as a function of airspeed, which is of concern to both the structural and aerodynamic analysis. Such redistribution can cause internal structural load and stress redistributions, as well as modify the stability and control derivatives. MSC.Nastran

computes the aircraft trim conditions, resulting in the recovery of structural responses, aeroelastic stability derivatives, and static aeroelasticity divergence dynamic pressures.

Static aeroelastic problems can be solved in a number of ways depending on the type of analysis required. In this study, three methods are used: rigid stability derivatives, restrained analysis for trim and stability derivative analysis, and unrestrained stability derivative analysis. Rigid stability derivative analysis can be used to examine the aeroelastic results. This type of analysis provides both splined and unsplined rigid stability derivatives, which can be compared to provide an assessment of the quality of the spline. If the numbers vary dramatically, this can indicate that not all of the aerodynamic elements have been joined to the structure. In addition, the rigid stability derivatives can be compared to both the restrained and unrestrained values. Large differences can indicate large structural deformations and may point to conditions such as local weaknesses in the structure, an aerodynamic model displaced from the structural model, or errors in the input of the flight condition. Restrained analysis is a simplified method where it is assumed that all of the supported degree of freedom terms can be neglected. Finally, unrestrained analysis requires the stability derivatives to be invariant with the selection of the support point location. This invariance is obtained by introducing a mean axis system. The deformations of the structure about this mean axis system are constrained to occur such that the center of gravity does not move. In addition, there is no rotation of the principal axes of inertia.

Control Surface Development

Traditional control surfaces were created using the MSC.FlightLoads interface. In this case, three different control surfaces were defined using aerodynamic panels and

examined for their effectiveness during roll. All three are located on the outboard portion (tip) of the wing, each with dimensions of $0.3c_t$ by $0.5S_{ob}$. In the first, the control surface is at the very tip of the wing, the second is in the middle of the outboard wing, and the last is located where the outboard wing meets up with the joint, as shown in Figures 3-7, 3-8, and 3-9, respectively.

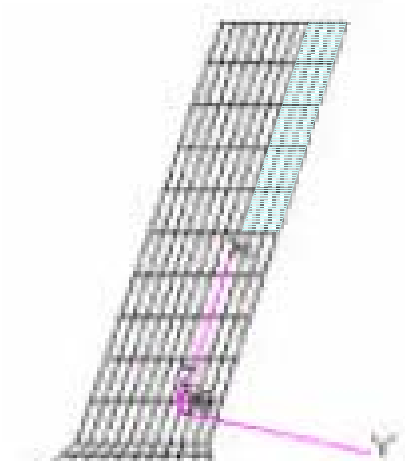

Figure 3-7: Control Surface for Roll, End of Tip

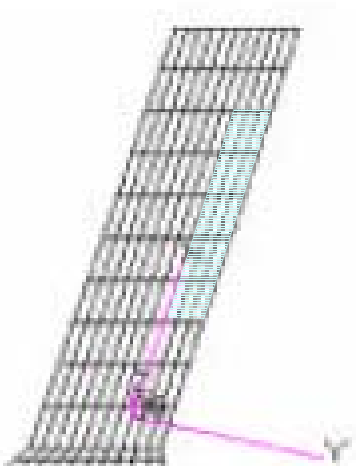

Figure 3-8: Control Surface for Roll, Middle of Tip

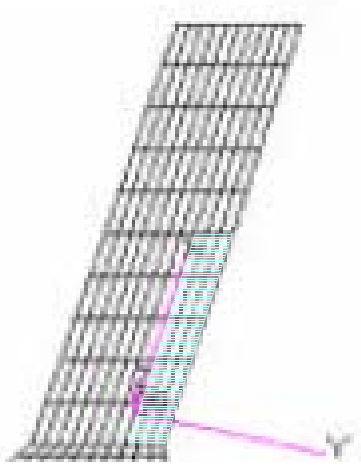

Figure 3-9: Control Surface for Roll, Root of Tip

The same method was used to define control surfaces for lift. For this condition, the control surfaces each had dimensions of $0.5c_{ra}$ by $0.5S_{ib}$ and were located on the aft wing rather than the tip.

MSC.Patran was used to define the boundary conditions of a linear structural model, which was then imported into MSC.FlightLoads. In MSC.FlightLoads an aerodynamic model, including the control surfaces shown above, was splined to the structural model. The resulting model was used to examine the effectiveness of each control surface. The first step was to identify at what flight condition, if any, the control surface reverses. This is done by simply identifying the dynamic pressure at which the nondimensional roll rate for each control surface crosses zero and becomes negative. The nondimensional roll rate is defined as $Pb/2V\delta_a$, where P is the roll rate, b the span, V the velocity, and δ_a is the control surface deflection, in this case set to ten degrees., and is plotted against the dynamic pressure to determine where reversal occurs.

Aft-wing Twist Using Scheduled Control Surfaces

To examine maneuver trim with aft-wing twist, and compare the trim to the PanAir results of Roberts, a series of ten control surfaces covering the entire aft wing (100% of the chord) was created manually in the MSC.Nastran bulk data code by Rasmussen [21]. The twist was simulated by linking the control surfaces so that the deflection of each surface was linearly dependent on the next inboard surface, as shown in Equation (3-13), where u^D is the dependent variable and u_i^I is the independent variable.

$$u_D = \sum_{i=1}^{n} C_i u_i^I = 0.0 \tag{3-13}$$

The free root panel was allowed to twist freely. The next panel was forced to twist at 90 percent of the first panel, and the panels continued in this pattern down the length of the aft wing (Figure 3-10). The model was then trimmed at each mission point using MSC.Nastran with the outputs providing trim results (angle of attack and twist angle) to compare to PanAir.

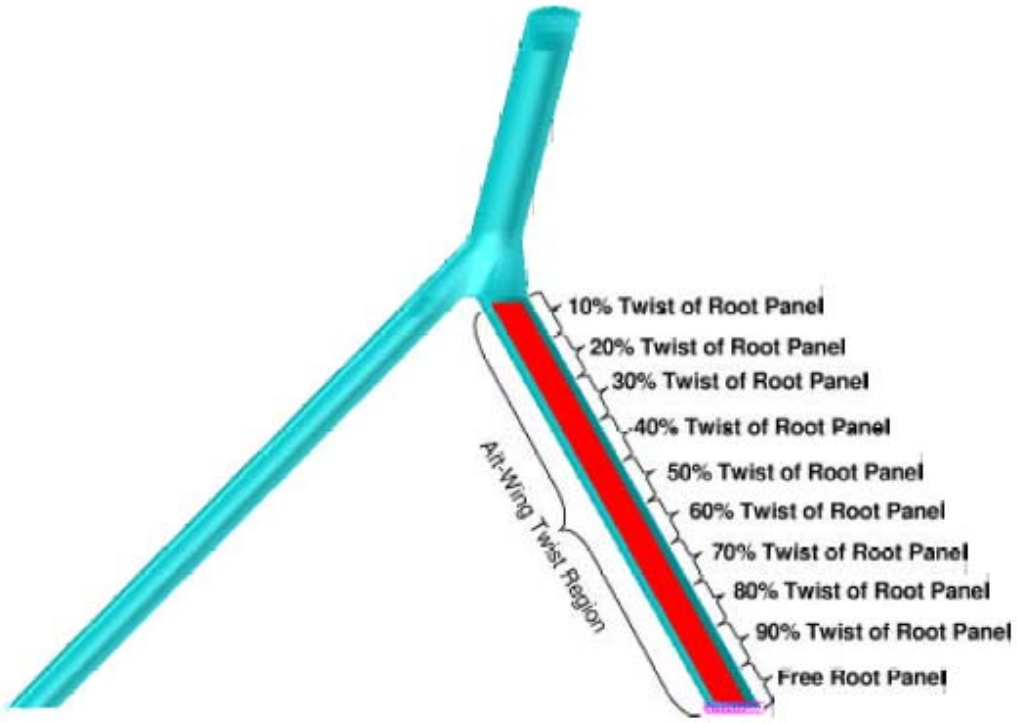

Figure 3-10: Linearly Tapered Aft-Twist Control Mechanism

Aft-Wing Twist Using MSC.Nastran

Another method to perform trim using aft wing twist was manual input into the MSC.Nastran bulk data. For this method, a single grid point is defined at the root of the aft wing in the center of the airfoil, and all the grid points at the root were made dependent on that point, as shown in Figure 3-11.

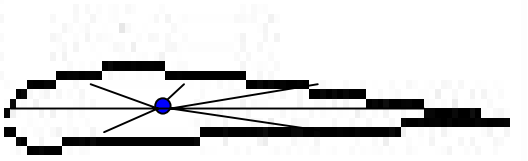

Figure 3-11: Grid Point Definition

The twist of this new grid point was defined as a control variable for trim, which would cause the grid points that define the airfoil to twist. This twist at the root is then carried through the entire aft wing via the spars, thus twisting the entire aft wing.

The twist was performed using a number of MSC.Nastran bulk data cards. The AEPARM card defines the general aerodynamic trim variable degree of freedom, which is derived from the AEFORCE input data. This card simply includes the controller name and the label used to describe the units of the controller values (NM for this effort). The UXVEC card specifies the vector of aerodynamic control point values by specifying the controller name. The twist, or moment, is programmed by defining a static concentrated moment at the grid point. The MOMENT card specifies the grid point and specifies the magnitude and a vector that determines the direction. For this case, the scale of the twist is set to 1.18E6, which is calibrated to equate to a twist deflection of one degree, and the vector is [0, 1, 0] (along the span). The AEFORCE card is then used to define a vector of absolute forces (not scaled by dynamic pressure) associated with a particular control vector. The force vector is defined on either the structural grid or aerodynamic mesh and is used in static trim. The card specifies the Mach number used (M = 0.5), the symmetry of the force vector in the XZ and XY planes (symmetric and asymmetric, respectively), the control parameter vector associated with this downwash vector (referenced from a UXVEC entry), the type of mesh used (structural grid), the MOMENT data (AFTWIST), and the magnitude of the aerodynamic extra degree of freedom (1.0). The bulk data for this model can be found in Appendix B.

IV. Results

Spline Examination

The first check of the fidelity of the model used in this study was an assessment of the quality of the spline. This can be determined by examining the rigid splined and unsplined stability and control derivatives. As discussed in Chapter III, if the numbers differ significantly, it may indicate that the aerodynamic forces may not have been transferred consistently to the structure. Since the aerodynamic mesh for this model was splined to the structural grid at only three chordwise locations for the fore and aft wings and four chordwise locations for the joint and tip, it is important to verify that the spline is complete. Table 4-1 gives an example of the splined and unsplined lift coefficient derivative with respect to control surface deflection for a series of dynamic pressures at mission point 2-98, 2.5g symmetric pullup maneuver (similar results were seen at other mission points). The two sets are very close, indicating the spline is satisfactory.

Table 4-1: Spline Analysis

	RIGID	
Q	UNSPLINED	SPLINED
0.01	2.483E+00	2.483E+00
500	2.538E+00	2.538E+00
1000	2.598E+00	2.597E+00
2000	2.731E+00	2.730E+00
3000	2.890E+00	2.890E+00
4000	3.085E+00	3.084E+00
5000	3.332E+00	3.332E+00
6000	3.664E+00	3.663E+00
7000	4.149E+00	4.148E+00
8000	4.920E+00	4.919E+00

Aerodynamic Force and Pressure Distributions

Force Distribution

The spanwise force distribution was calculated at the beginning and end of the mission (mission points 0-00 and 2-98) for the aft wing, fore wing, joint, and outboard tip. The forces were calculated at each individual aerodynamic box, and then summed chordwise. These summed forces were then plotted along the span, with location one at 10 percent of the wing section span (from the most inboard location), location two at 20 percent of the wing section span, and so forth. Figures 4-1 and 4-2 show the 2.5g load factor lift force distribution for the aft wing, fore wing, joint, and outboard tip at mission point 0-00 for the PanAir and MSC.Nastran models, and Figures 4-3 and 4-4 show the distribution for mission point 2-98 for the PanAir and MSC.Nastran models, respectively. As would be expected, the shape of the lift distribution is the same at each mission point, with 2.5 times more lift required for the full fuel condition (60% fuel fraction). The size of the spanwise cuts in the joint and tip differ from each other and the fore and aft wings, explaining the discontinuity in magnitude across these wing segments.

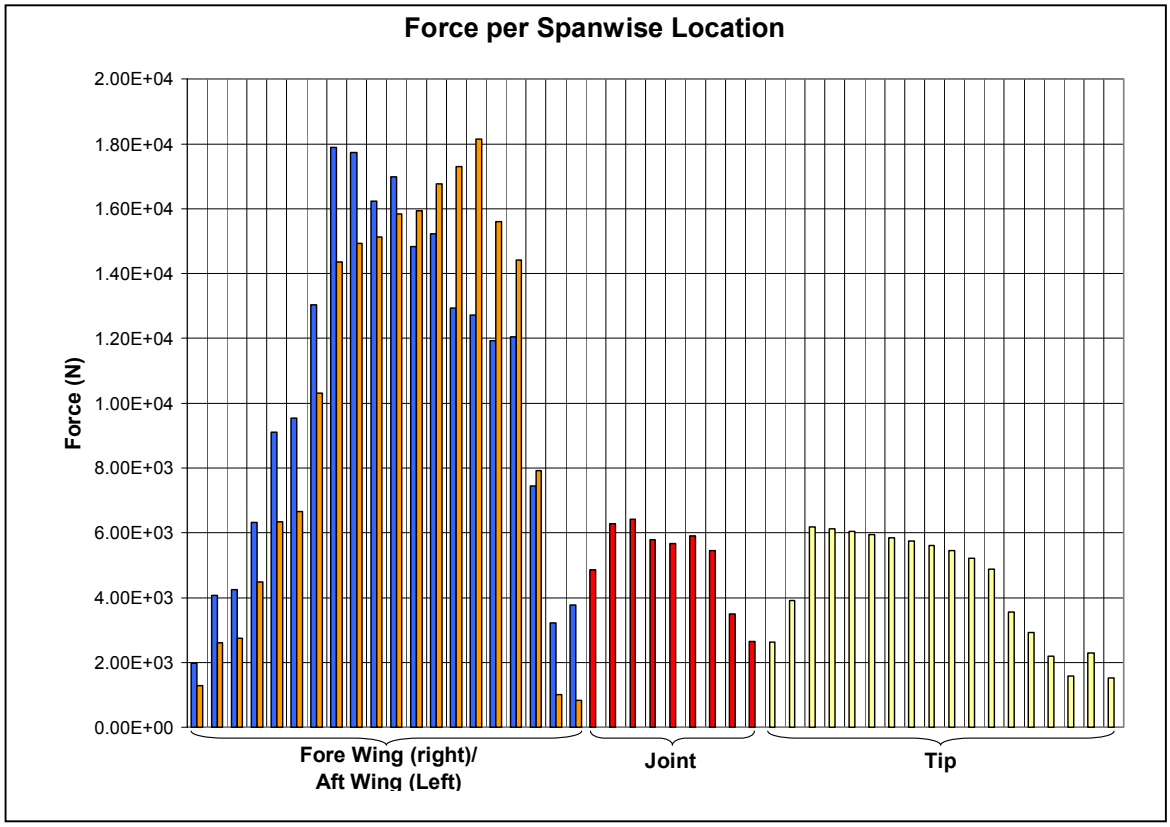

Figure 4-1: PanAir Force per Spanwise Location, Mission Point 0-00

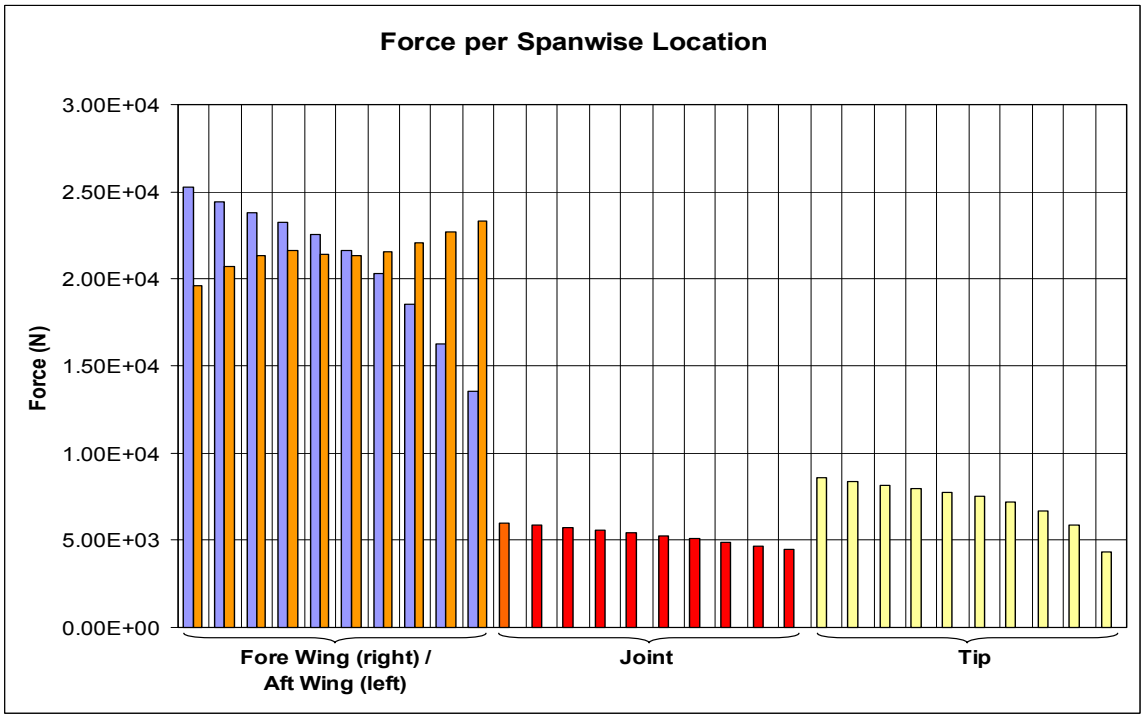

Figure 4-2: MSC.Nastran Force per Spanwise Location, Mission Point 0-00

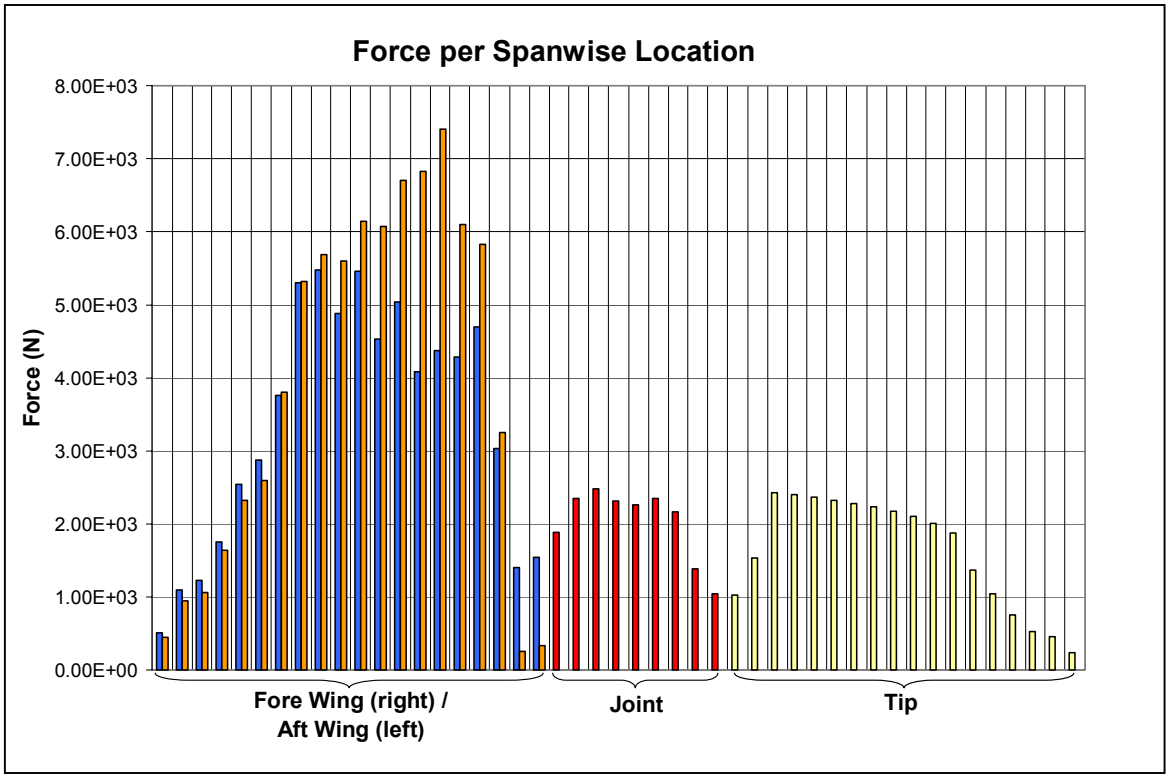

Figure 4-3: Patran Force per Spanwise Location, Mission Point 2-98

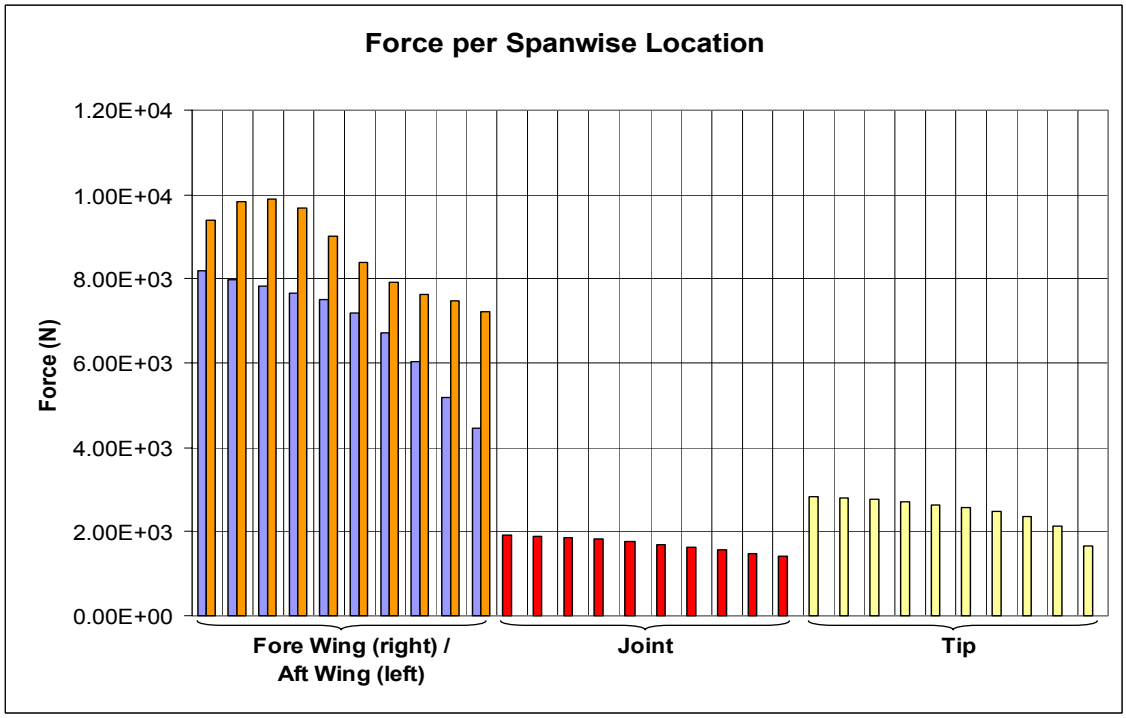

Figure 4-4: MSC.Nastran Force per Spanwise Location, Mission Point 2-98

The ratio of the percentage of lift per wing section was also calculated, as shown in Table 4-2. As expected, the majority of the lift is experienced in the aft and fore wings, the panels with the largest surface areas. As we go through the mission profile, the percentage of lift on the fore wing increases. The center of gravity moves forward as fuel is consumed, demanding that more of the total lift be carried by the fore wing. The outboard tip carries more lift than the joint, because the joint has a larger surface area and a experiences less interference from the other aerodynamic panels.

Table 4-2: Percentage of Total Lift per Aerodynamic Panel

Mission Point	Aft Wing 63.5 m^2 (38%)	Fore Wing 63.5 m^2 (38%)	Joint 18.8 m^2 (11%)	Outboard Tip 21.7 m^2 (13%)
0-00	38%	39%	10%	13%
2-98	35%	44%	9%	13%

Running Loads

The running loads and pressures were then plotted using a similar method as described above. The running loads were calculated by summing the pressures at the aerodynamic boxes chordwise, and the plotting them spanwise. Figures 4-5 and 4-6 show the spanwise running loads for the aft wing, fore wing, joint, and outboard tip at mission points 0-00 and 2-98, respectively.

The running loads are essentially continuous along the span. The sum of the loads for the most outboard points of the fore and aft wing equal the load at the most inboard point of the joint. The load then runs continuously from the joint to the outboard tip.

Figure 4-5: Running Loads, Mission Point 0-00

Figure 4-6: Running Loads, Mission Point 2-98

Pressure Distribution

The pressure distribution was plotted for the leading edge, quarter chord, half chord, three quarter chord, and trailing edge of each aerodynamic panel for mission segments 0-00 and 2-98, as shown in Figures 4-7 through 4-14. For both mission segments, the distribution is elliptical for the aft wing and outboard tip, but shows a unique distribution for the joint and fore wing. The unusual curve shape at the joint may be due to the way the joint is modeled. At the most inboard portion of the joint, the cross-section has an airfoil shape that is then blended along the span of the joint. It maintains the same shape at the most outboard cross section, just for a shorter chord length. The unusual shape for the fore wing pressure distribution at mission point 0-00 is more difficult to explain. It was originally considered to be a result of the flexible twist of the fore wing, but further studies did not validate that. It may be due to interactions between the fore wing and the joint, but more analysis is required beyond the scope of this study.

From beginning to end of mission, the leading edge pressure distribution decreases significantly. This is the result of a smaller angle of attack required to trim the vehicle at a lighter weight, as fuel is burned.

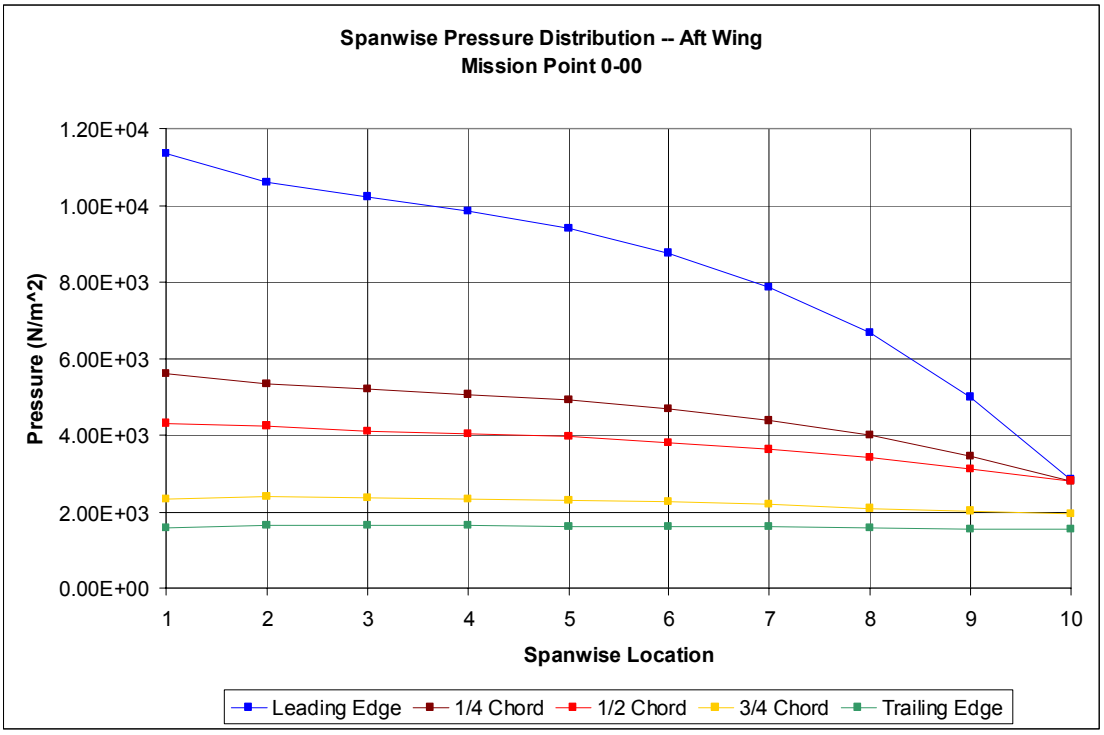

Figure 4-7: Aft Wing Pressure Distribution, Mission Point 0-00

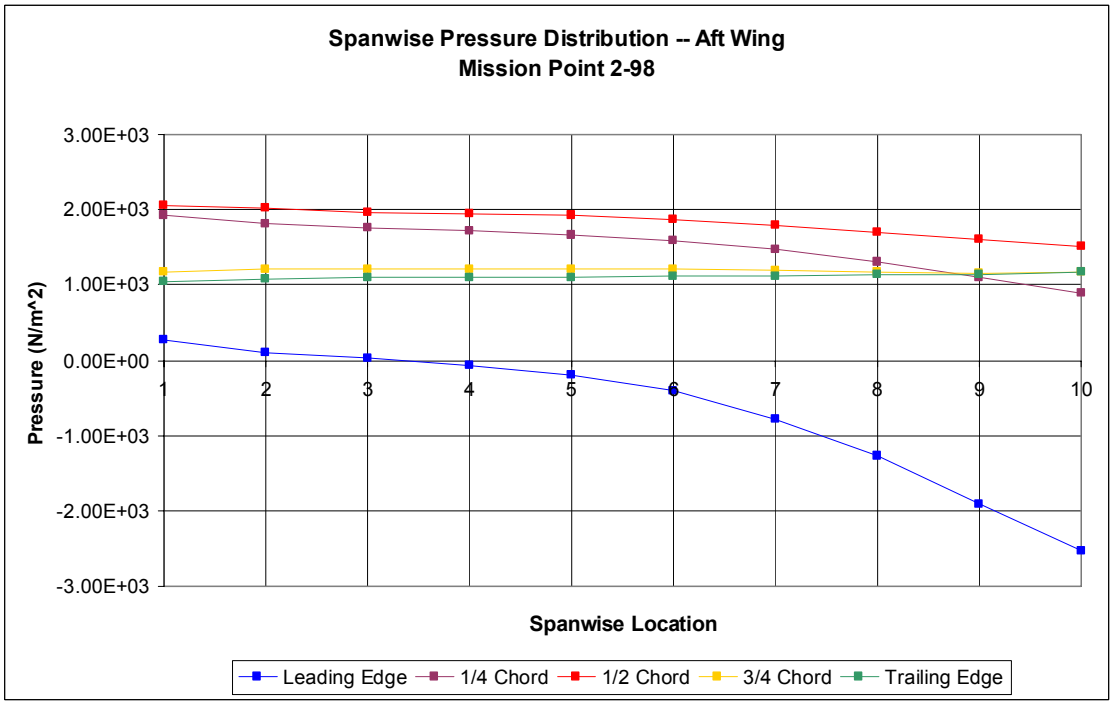

Figure 4-8: Aft Wing Pressure Distribution, Mission Point 2-98

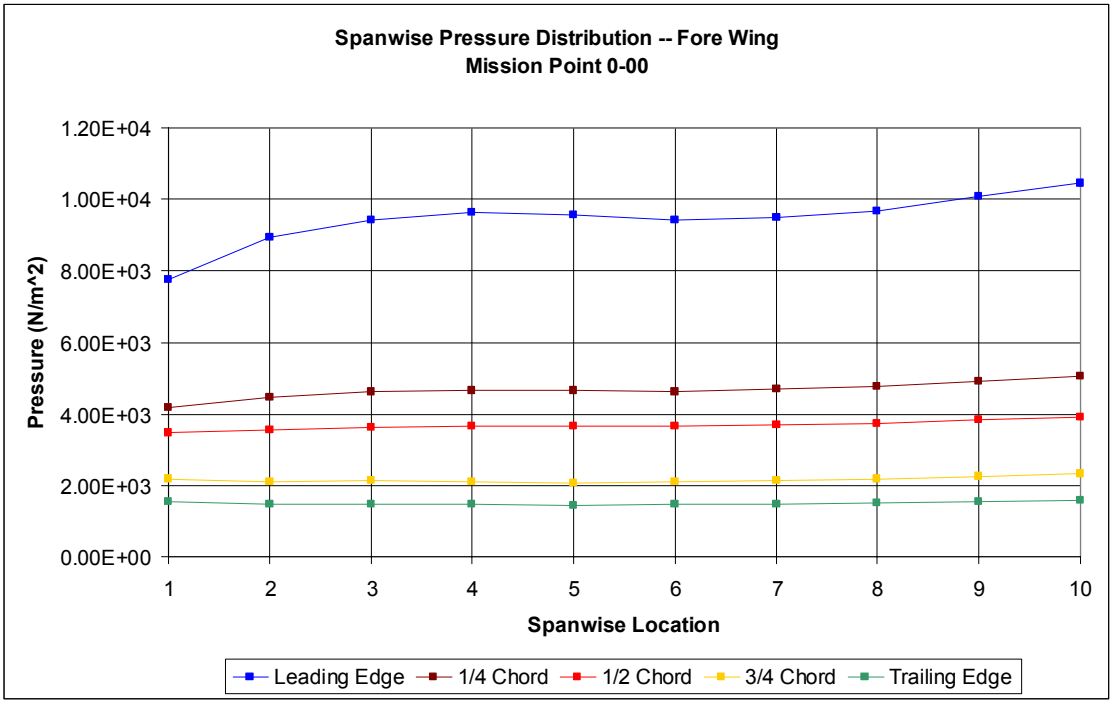

Figure 4-9: Fore Wing Pressure Distribution, Mission Point 0-00

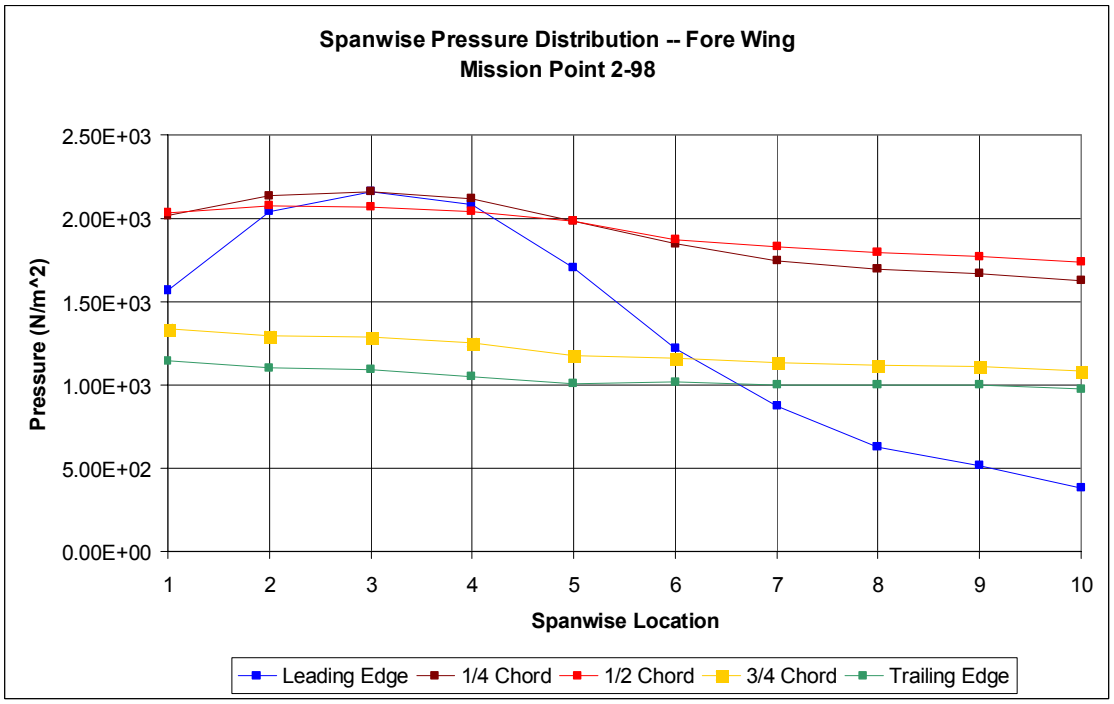

Figure 4-10: Fore Wing Pressure Distribution, Mission Point 2-98

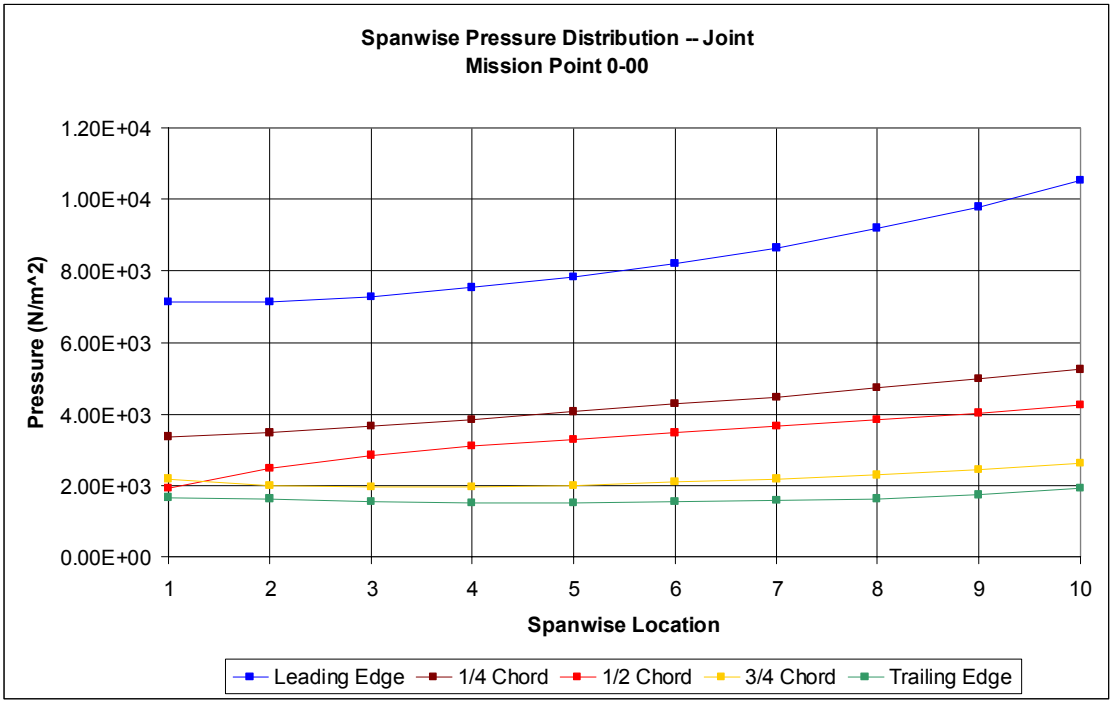

Figure 4-11: Joint Pressure Distribution, Mission Point 0-00

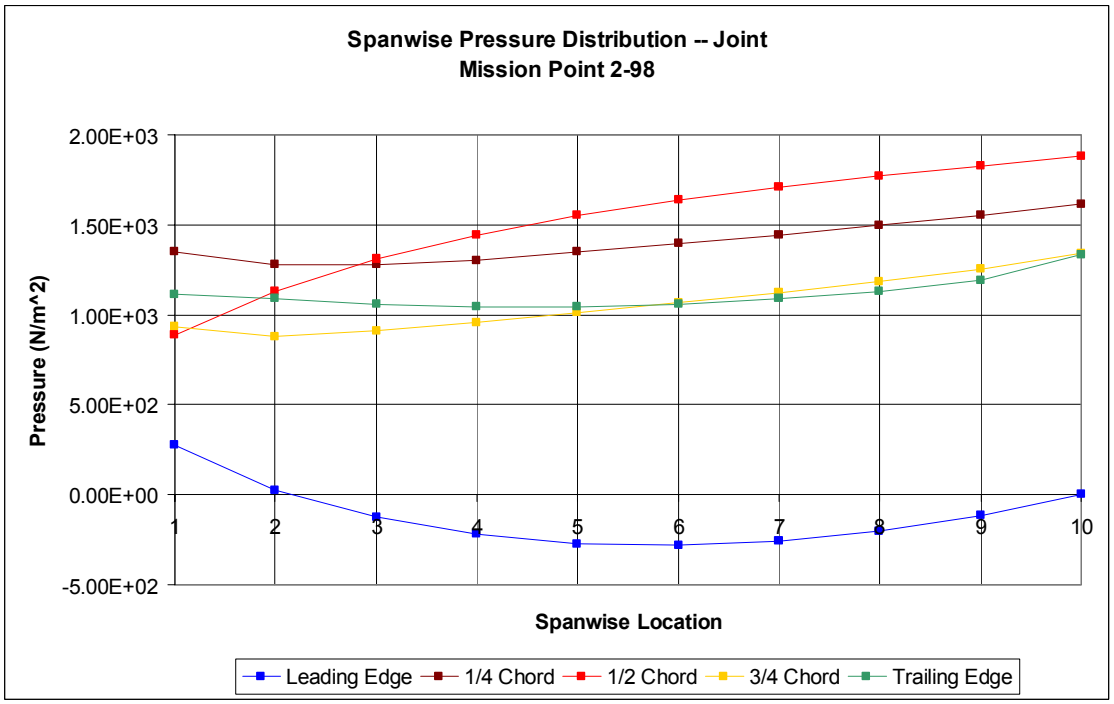

Figure 4-12: Joint Pressure Distribution, Mission Point 2-98

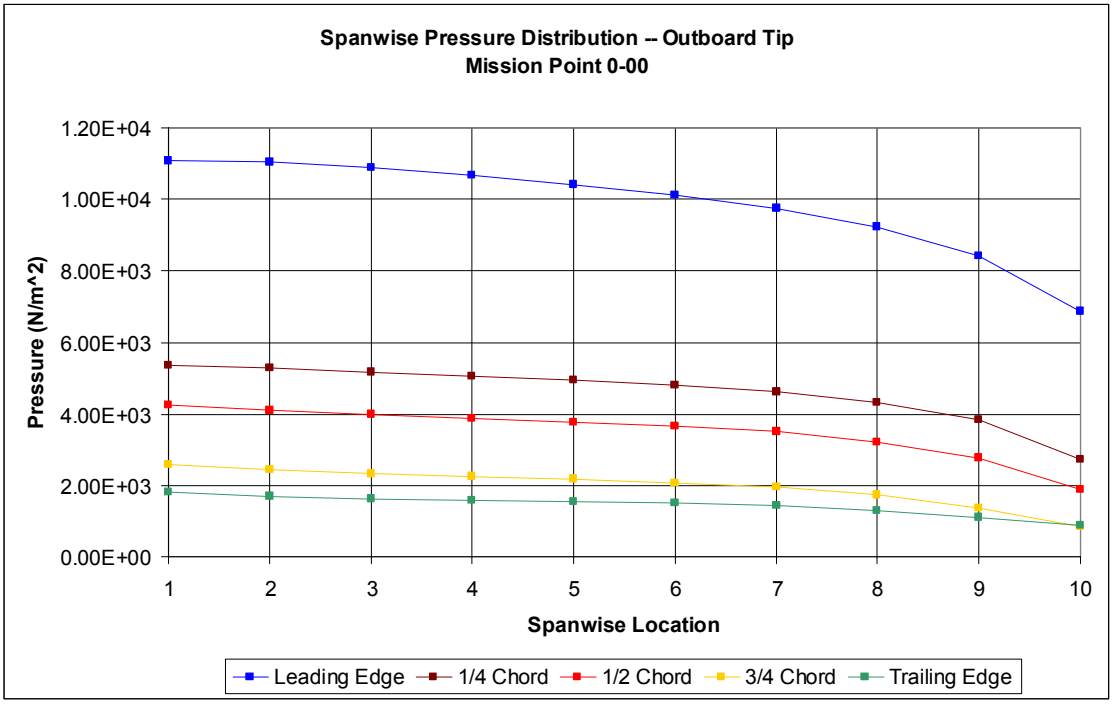

Figure 4-13: Outboard Tip Pressure Distribution, Mission Point 0-00

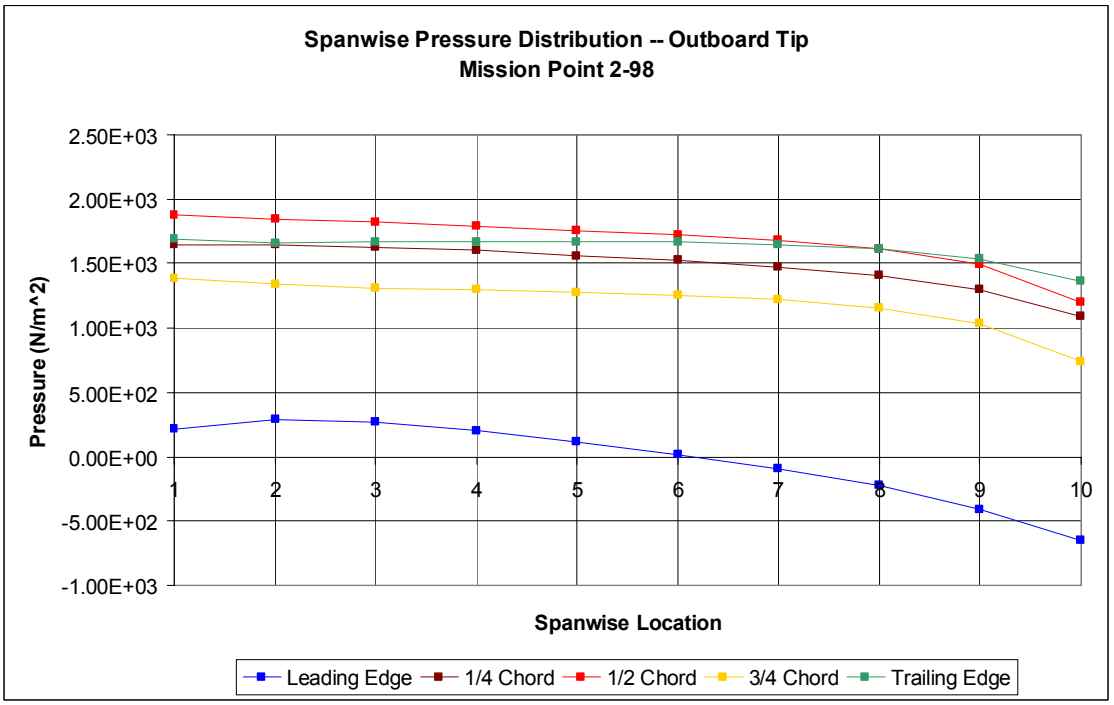

Figure 4-14: Outboard Tip Pressure Distribution, Mission Point 2-98

Control Surfaces

Roll

To examine the effect of surfaces to control roll and lift of the joined-wing, control surfaces were created on the tip and the aft wing, respectively. For this effort, two different models were examined. The first was the preliminary structural design used by Roberts, developed using both linear (light model, 11,360 kg at mission point 2-98) and non-linear (heavy model, 17,388 kg at 2-98) structural analysis. The second was an updated model (15,646 kg at 2-98), designed using a more realistic stress allowable and developed using only linear structural analysis.

The preliminary model was examined at the end of mission, mission point 2-98. A constant altitude of 50,000 feet was assumed, and the nondimensional roll rate was examined as a function of the dynamic pressure, q. The nondimensional roll rate per unit control surface deflection is defined as $pb/2V\delta_a$, where p is the roll rate, b the span, V the velocity, and δ_a is the control surface deflection, in this case set to ten degrees. Figures 4-15 and 4-16 show the roll rate for each control surface of the light model and heavy model respectively.

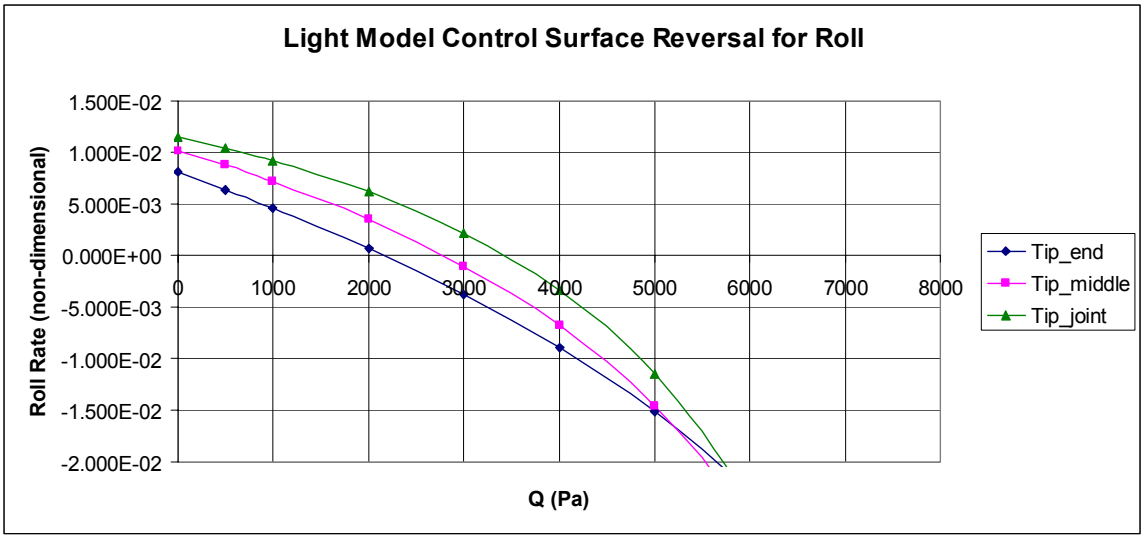

Figure 4-15: Light Model Control Surface Reversal for Roll

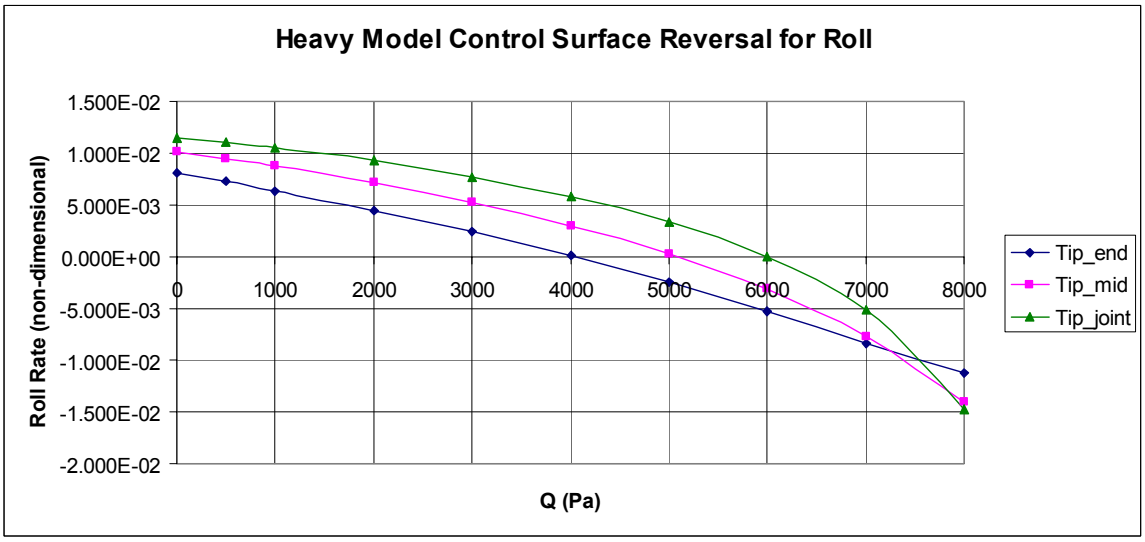

Figure 4-16: Heavy Model Control Surface Reversal for Roll

Both the light and heavy models show that the most inboard control surface on the outboard tip is the most effective for roll – it reverses at a higher dynamic pressure. The control surfaces for both the light and heavy models show reversal above the cruise and

loiter speeds at 50,000 feet, but within the flight envelope when flying above Mach = 0.3 at sea level.

The updated model was examined at mission point 2-98 at an altitude of 50,000 feet and at sea level. For reference, Table 4-3 shows how Mach number varies with dynamic pressure at the two altitudes. The roll rate for each control surface was examined, as shown in Figures 4-17 and 4-18. For this model, none of the control surfaces for roll even approach reversal. As the dynamic pressure q increases, the roll rate does decrease for both situations, but more quickly at the higher altitude. This difference in rate of change is a result of the lower density at 50,000 feet, and therefore higher Mach numbers at higher altitudes. Lower roll rates at higher velocities indicate a loss of roll effectiveness due to the flexible twist of the wings. The climb in roll rate at the highest dynamic pressures for the 50,000 foot case is unusual, and may be caused by a transition from a subsonic to a supersonic analysis.

Table 4-3: Mach Number at Altitude

Q	Mach at 50,000 ft	Mach sea level
0.01	0.001	0.000
1000	0.351	0.119
2000	0.496	0.168
3000	0.608	0.206
4000	0.702	0.237
5000	0.785	0.265
6000	0.86	0.291
7000	0.929	0.314
8000	0.993	0.336

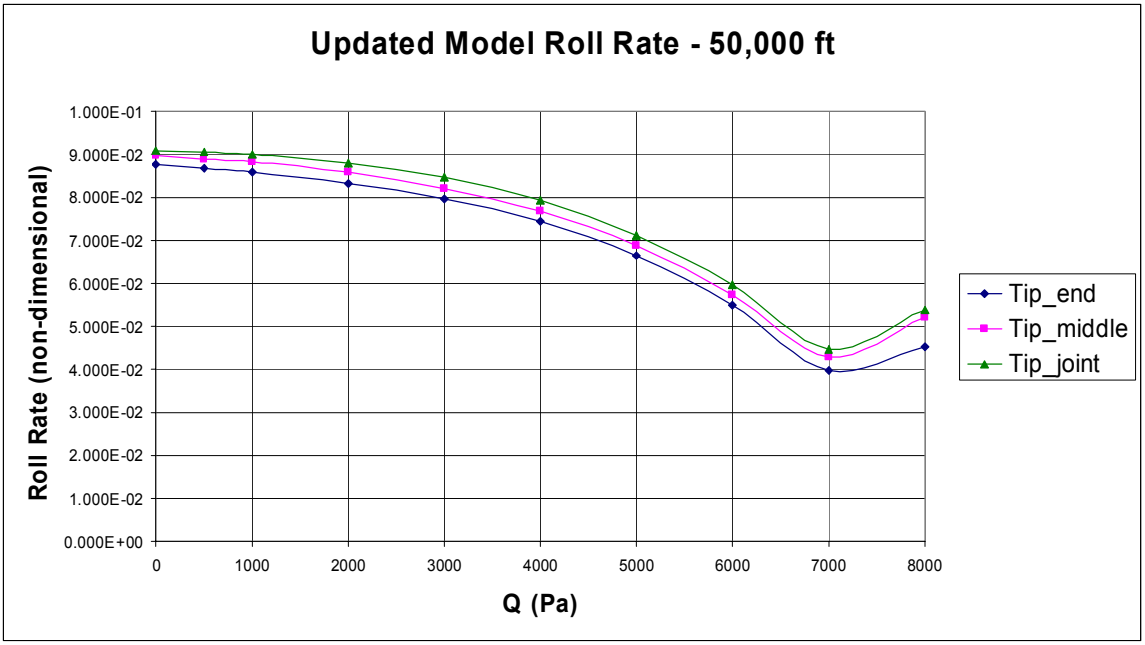

Figure 4-17: Updated Model Roll Rate at 50,000 ft

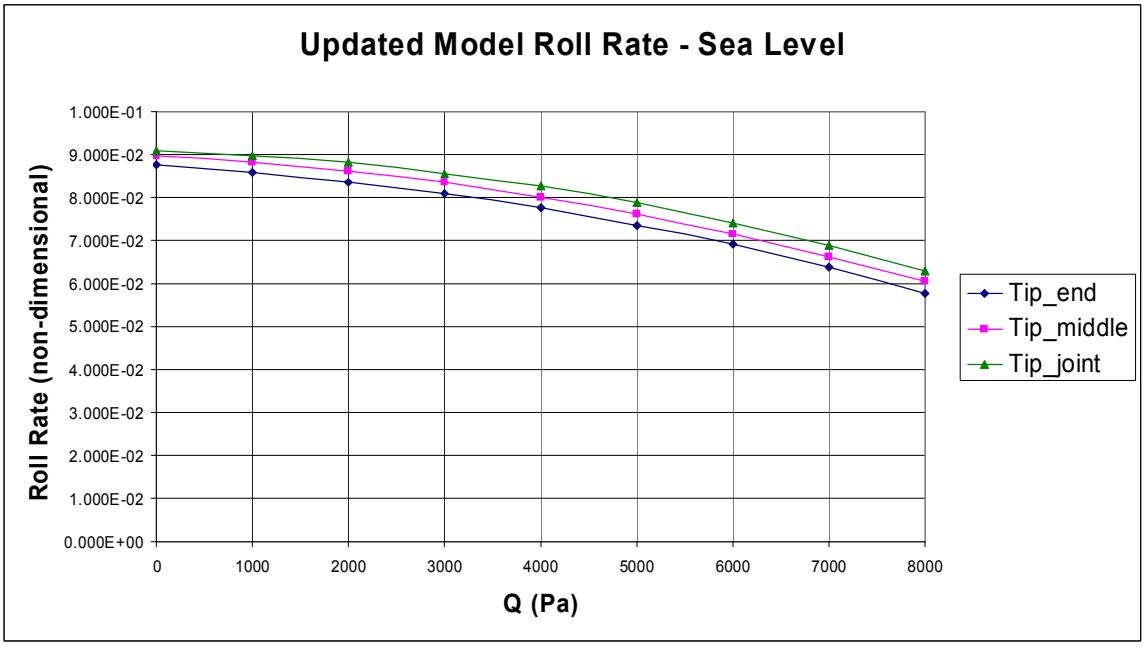

Figure 4-18: Updated Model Roll Rate at Sea Level

Lift

Camber effects were used in all the analyses, but are particularly important to include in lift effectiveness. The results achieved in PanAir are based on an airfoil where the zero-lift angle of attack is $\alpha_0 = -4$ degrees, but the aerodynamic model developed in MSC.FlightLoads uses aerodynamic flat plates. Therefore, information regarding the airfoil camber of the LRN-1015 airfoil was added directly into the MSC.FlightLoads model (Appendix A), resulting in an $\alpha_0 = -3.3$ degrees. Three control surfaces were defined on the aft wing in the same fashion as those used for roll on the tip. The restrained and unrestrained control surface effectiveness for the original model are plotted as shown in Figures 4-19 and 4-20 and Appendix C respectively, where the control surface effectiveness ε is defined as the change in lift due to a unit deflection of the control surface for the flexible model over the change in lift due to a unit deflection of the control surface for the rigid model. The restrained analysis determines the flexible stability derivatives for deflections relative to the support point location, while the unrestrained analysis determines flexible stability derivatives for deflections relative to a mean axis that maintains invariant inertia properties.

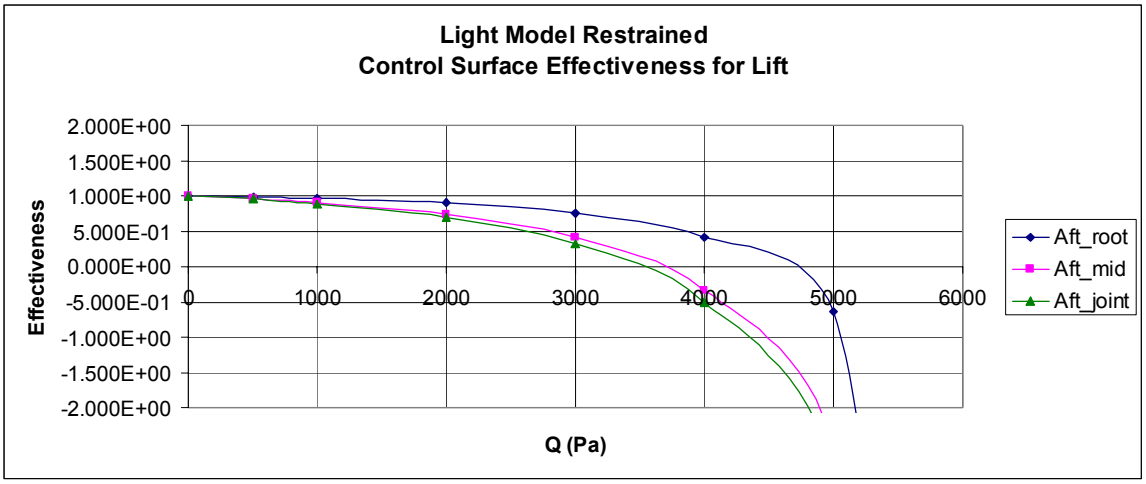

Figure 4-19: Light Model Restrained Control Surface Effectiveness for Lift

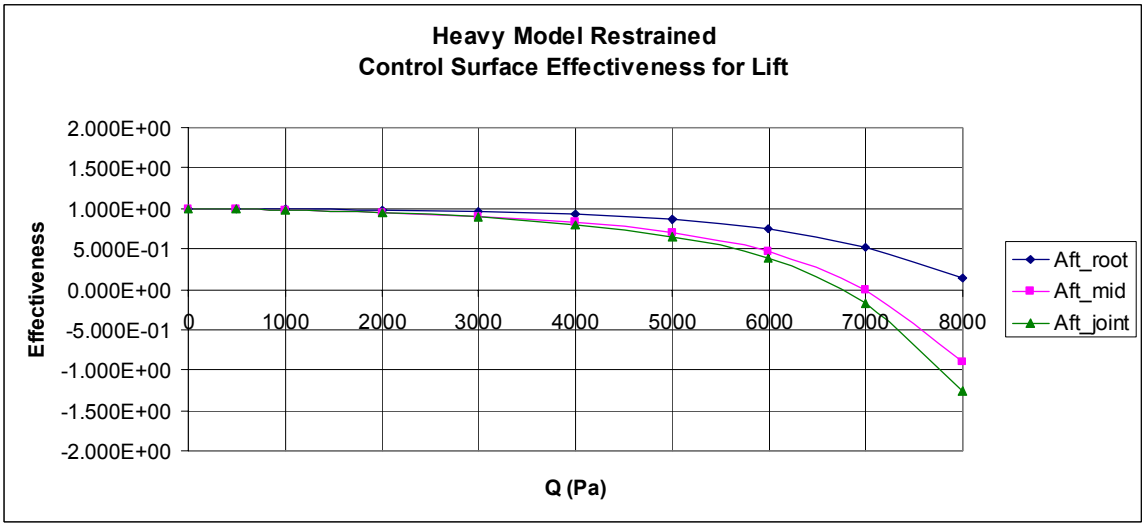

Figure 4-20: Heavy Model Restrained Control Surface Effectiveness for Lift

For the heavy model, the effectiveness appears approximately constant within the flight regime, while it decreases relatively rapidly for the light model. An examination of the effectiveness for heavy model (Figure 4-20), however, shows that while the effectiveness stays above 80% within the flight regime, it decreases rapidly after q = 4000 Pa. The light model begins to show dramatic variation at higher values of dynamic

pressure. The heavy model maintains a reasonable effectiveness for all values of dynamic pressure, except for the drop that begins around q = 7500 Pa for the unrestrained model (see Appendix C).

The same method was used for the updated model, and the results were examined at both 50,000 feet altitude and sea level, as shown in Figures 4-21 and 4-22. The updated model does not show any of the control surface reversal seen in the original model. As expected, the control surfaces located at the most inboard positions were the most effective

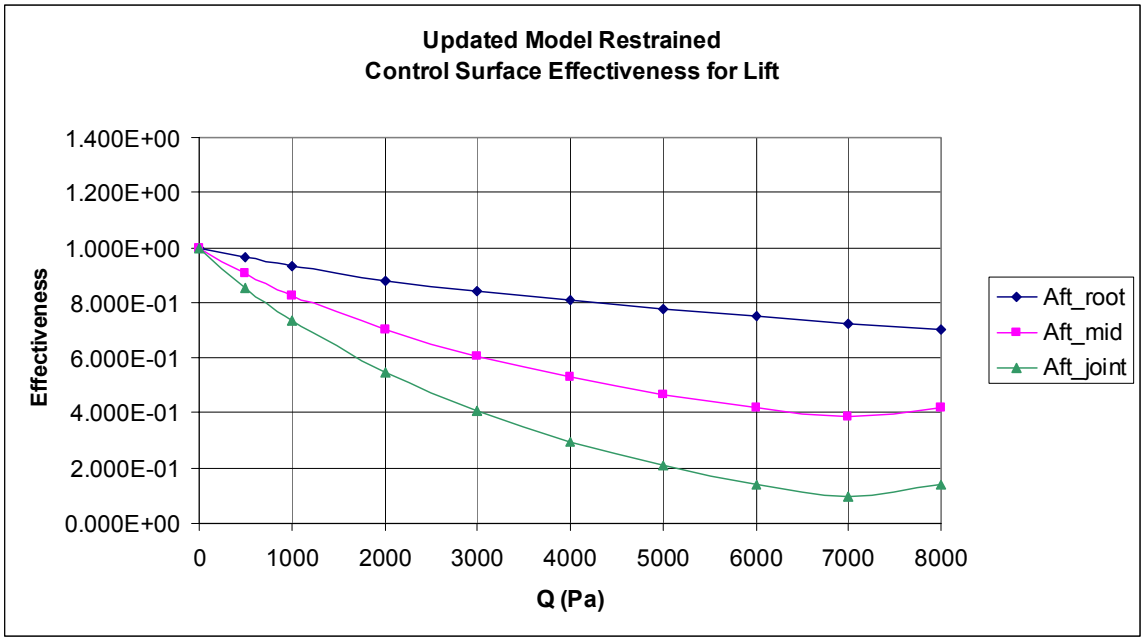

Figure 4-21: Restrained Aft-Wing Control Surface Effectiveness at 50,000 ft

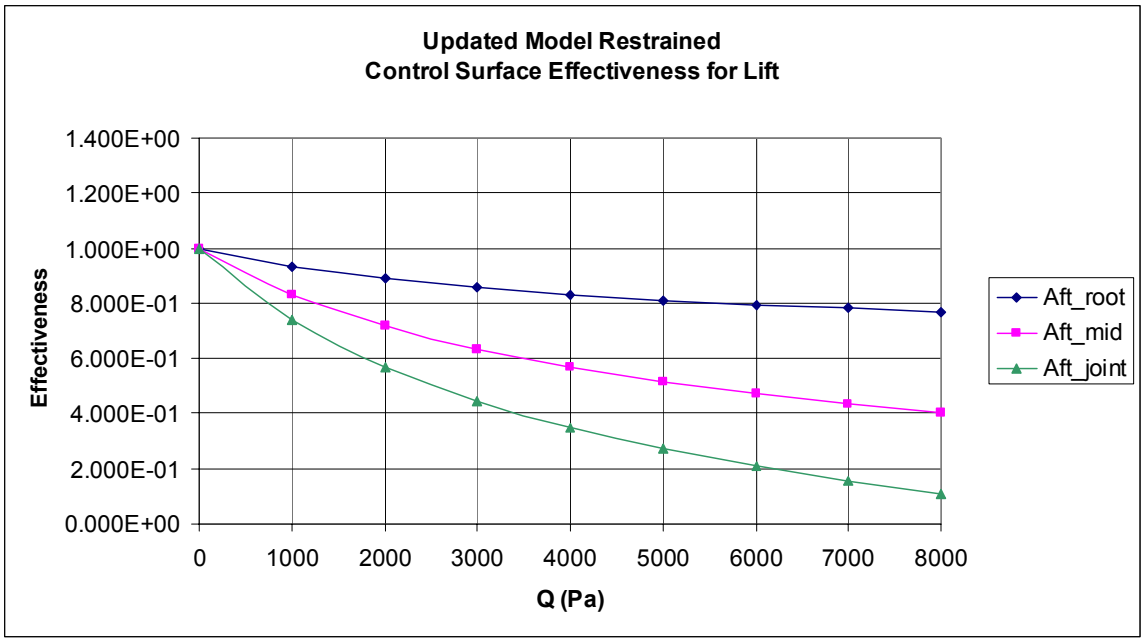

Figure 4-22: Restrained Aft-Wing Control Surface Effectiveness at Sea Level

Scheduled Aft Wing Aerostructural Results

2.5G Load Case

To examine aft-wing twist and compare the trim to the PanAir results of Roberts, a series of ten control surfaces covering the entire aft wing was created manually in the MSC.Nastran bulk data code. The twist was simulated by linking the control surfaces so that the deflection of each surface was dependent on the next inboard surface. The most inboard surface was independent, as was the angle of attack. MSC.Nastran was then run, with the outputs providing trim results (angle of attack and twist angle) to compare to PanAir. Roberts' results are shown in Table 4-4, the results of this study in Table 4-5.

Table 4-4: PanAir Flexible Trim Results [1]

Mission Point	aoa (degrees)	twist (degrees)	cg x location (m)
0-00	8.227	-0.90885	14.362
0-50	7.105	-1.35890	14.351
1-00	17.933	-4.25450	14.336
1-50	12.735	-5.14131	14.292
2-00	1.141	-0.48657	14.211
2-50	0.758	-3.64127	14.184
2-98	0.265	-3.80787	14.152
2-98-gc	0.200	-0.48170	14.152
2-98-gb	1.216	-0.20542	14.152

Table 4-5: MSC.Nastran Flexible Trim Results – Scheduled Aft Wing

Mission Point	aoa (degrees)	twist (degrees)	cg x location (m)
0-00	9.520	-8.615	14.243
0-50	8.435	-3.792	14.219
1-00	20.903	-3.005	14.189
1-50	14.309	-4.087	14.100
2-00	3.095	-2.770	13.930
2-50	2.637	-2.682	13.873
2-98	2.259	-5.619	13.811
2-98-gc	-2.000	4.856	13.811
2-98-gb	-2.298	2.244	13.811

The angle of attack required to trim the aircraft between the two models is off by approximately one or two degrees at each mission point. This may be the result of the differences in aerodynamic theory between PanAir and MSC.Nastran, the difference in center of gravity location between the two models, or the different twist mechanisms used. One difference in the aerodynamic theories is the calculation of the zero-lift angle of attack. The zero-lift angle of attack of the LRN-1015 airfoil is -4^{o}. The camber is

manually included in the MSC.Nastran model, creating a zero-lift angle of attack of -3.3°. AVTIE and MSC.Nastran also calculate the center of gravity location differently, as shown in Tables 4-4 and 4-5. AVTIE calculates the location based on the geometry model, whereas MSC.Nastran uses mass properties of the finite elements.

Note that for each mission segment (ingress, loiter, and egress), the angle of attack required to trim decreases throughout the segment. As the aircraft continues through each segment, its overall weight decreases as fuel as consumed. The lighter aircraft does not need to create as much lift to counteract the weight, so the angle of attack decreases.

With the exception of the first mission point, the MSC.Nastran twist is differs from the PanAir twist by 1-2 degrees. The difference is at least partially due to the different center of gravity locations between the two models and the different twist mechanisms used by the two programs. The expected trend would be for the twist angle to decrease throughout each mission segment with the angle of attack, as it does for the PanAir results.

Cruise and Turbulent Gust

To compare MSC.Nastran gust results to PanAir, it was assumed that the aircraft was flying straight and level, 1.0G cruise and then experienced a cruise gust of 50 ft/s and a turbulent gust of 66 ft/s at a flight speed at least 43 knots slower than cruise velocity. This was modeled by first trimming the vehicle for 1.0G cruise to determine the angle of attack and twist angle. The angle of attack for gust was then calculated by adding the 1.0G trim angle to the change in angle of attack due to the vertical gust. This new angle of attack and the trim twist angle were set, and the aircraft was then analyzed to

determine load factor and pitch rate, resulting in the values found in Table 4-6. Table 4-7 shows the results from Roberts [1].

Table 4-6: MSC.Nastran Gust Results

Nastran Results						
Gust Condition	1 G Trim Twist (deg)	1 G Trim AoA (deg)	Change in AoA (deg)	Gust AoA (deg)	Load Factor	Pitch Acceleration
Cruise Gust	4.85600	-2.283	3.106	0.823	3.74	0.118
Turbulent Gust	2.24400	-2.298	4.296	1.998	3.53	0.165

Table 4-7: PanAir Gust Results

PanAir Results					
Gust Condition	1 G Trim Twist (deg)	1 G Trim AoA (deg)	Change in AoA (deg)	Gust AoA (deg)	Load Factor
Cruise Gust	-0.48170	-2.906	3.106	0.200	2.795
Turbulent Gust	-0.20542	-3.080	4.296	1.216	2.911

For the MSC.Nastran gust results, the load factor for the cruise gust condition is higher than that for the turbulent gust condition. This is the result of analyzing the cruise gust condition at a higher dynamic pressure, which requires more aft wing twist and therefore a higher load factor. The PanAir results show the opposite trend for load factor, which does not match those results and requires further analysis.

Aft Wing Twist Aeroelastic Results

The results in Table 4-8 were obtained in the same manner as the 2.5G Load Case above, using the model where the aft wing twists flexibly without the use of control surfaces (see the *Aft Wing Twist Using MSC.Nastran* section of Chapter III). The angle of attack results are significantly lower than those calculated for the scheduled aft wing twist model, but they do follow the same basic trend throughout the mission profile. The twist results, however, appear anomalous, and further study is required to investigate the cause.

Table 4-8: Nastran Flexible Trim Results –Aft Wing Twist

Nastran Results			
Mission	aoa	twist	cg
0-00	5.050	-1.062	14.243
0-50	4.020	-1.058	14.219
1-00	16.155	-1.050	14.189
1-50	9.512	-1.066	14.100
2-00	-1.227	-1.038	13.930
2-50	-1.678	-1.037	13.873
2-98	-2.073	-1.035	13.811

V. Conclusions and Recommendations

Conclusions

This study provided a comparison of PanAir results to MSC.FlightLoads results for a joined-wing SensorCraft. Specifically, the aerodynamic load distribution and flexible aerodynamic trim were examined. The aerodynamic trim looked at two cases, scheduled aft wing twist and flexible aft wing twist.

This study also examined the effectiveness of control surfaces for the aircraft. Control surfaces for both roll and lift were developed, and their effectiveness was examined for the original light and heavy models and the updated model with the correct stress allowable.

Aerodynamic Load Distribution

The comparison of aerodynamic load distribution for PanAir and MSC.FlightLoads shows that the distribution is essential the same for both models. The variations in the force distribution plots are explained by the differences in the mesh between the two models. They both show the same unexpected distribution for the fore wing, which may be the result of interactions between the fore wing and the joint. The spanwise running loads and pressure distribution show the expected results, with the same fore wing exception.

Control Surface Analysis

This study demonstrated the use of control surfaces on the outboard tip for roll and on the aft wing for lift. The locations of the control surfaces for roll are of particular concern, as for the original light model they can reverse within the flight regime. Lift

effectiveness was also examined, and is reasonable for all models within the flight regime. In fact, the lift effectiveness for the updated model never goes below zero in the subsonic regime.

Scheduled Aft Wing Twist

The scheduled aft wing twist model allows traditional modeling by scheduling control surfaces along the aft wing. The trim results show multiple differences between the PanAir and MSC.Nastran models. As the aircraft moves through the mission profile, the x location of the center of gravity moves forward, although the locations are not the same between the two models. This may be one reason for the differences in the calculated twist results. Another may be that the aerodynamic panel methods used by the two programs are different, including their consideration of the zero-lift angle of attack. Despite the differences in center of gravity location and twist, the angle of attack results are reasonable – they decrease throughout each mission segment as the aircraft burns fuel and requires less lift.

For the gust condition, the load factors differ between the PanAir and MSC.FlightLoads results. The load factor calculated by MSC.FlightLoads the cruise gust condition is larger than that calculated for the turbulent gust condition. This is expected due to the larger dynamic pressure used to analyze the cruise gust condition. The PanAir results must be examine further to validate that they used the same values for Mach number and dynamic pressure.

Flexible Aft Wing Twist

Flexible aft wing twist provides a more physically accurate model of the actual aircraft by twisting the aft wing at the root and allowing the structure to carry that twist

through the aerodynamic panel. The results for this study show that the trimmed angle of attack using flexible twist, while of a smaller magnitude, follows the same trends seen in the PanAir and scheduled aft wing twist models. The trimmed twist angle, however, seems to be essentially constant throughout the mission profile. This does not follow the previous studies and must be studied further to determine why.

Recommendations

Future efforts should take a number of issues into account. The first is to ensure an adequate spline between the structural and aerodynamic models, as demonstrated in this effort. Also, when including camber into the flat plate model, it is important to take into consideration the unusual cross section of the joint where it joins the fore and aft wings. At this location, it experiences the camber from the fore wing, an area of no camber, and then the camber of the aft wing. This shape then smoothes out along the joint spanwise, until it matches with the camber of the outboard tip.

Further investigation is required into the feasibility of modeling aft wing twist using the methods described at the end of Chapter III. This is a relatively new way of examining the use of an entire lifting surface as a control surface, and there is more work to be done. In addition, computational fluid dynamics should be used to provide a 3-D validation of the 2-D panel method results found to date.

A. Camber Bulk Data Inputs

Header Entry Format:

DMIJ	NAME	"0"	IFO	TIN	TOUT	POLAR		NCOL

Column Entry Format:

DMIJ	NAME	GJ	CJ		G1	C1	A1	B1
	G2	C2	A2	B2	~ etc. ~			

NAME	Name of the matrix
IFO	Form of the matrix being input 1 = Square 9 or 2 = Rectangular 6 = Symmetric
TIN	Type of matrix being input 1 = Real, single precision 2 = Real, double precision 3 = Complex, single precision 4 = Complex, double precision
TOUT	Type of matrix being created 0 = Set by precision system cell 1 = Real, single precision 2 = Real, double precision 3 = Complex, single precision 4 = Complex, double precision
POLAR	Input form of Ai, Bi (Integer = blank or 0 indicates real, imaginary format)
NCOL	Number of columns in a rectangular matrix
GJ	Grid, scalar or extra point identification number for column index
CJ	Component number for grid point GJ
Gi	Grid, scalar or extra point identification number for row index
Ci	Component number for GI for a grid point
Ai, Bi	Real and imaginary (or amplitude and phase) parts of a matrix element. If the matrix is real, the Bi must be blank

DMIJ	W2GJ	0	9	1	0	0		1
DMIJ	W2GJ	1	1		100001	3	-0.157922	
	100002	3	-0.079125		100003	3	-0.042589	
	100004	3	-0.013769		100005	3	0.01898	
	100006	3	0.06182		100007	3	0.10369	
	100008	3	0.10569		100009	3	0.0922	
	100010	3	0.15789		100011	3	-0.157922	
	100012	3	-0.079125		100013	3	-0.042589	

	100014	3	-0.013769		100015	3	0.01898	
	100016	3	0.06182		100017	3	0.10369	
	100018	3	0.10569		100019	3	0.0922	
	100020	3	0.15789		100021	3	-0.157922	
	100022	3	-0.079125		100023	3	-0.042589	
	100024	3	-0.013769		100025	3	0.01898	
	100026	3	0.06182		100027	3	0.10369	
	100028	3	0.10569		100029	3	0.0922	
	100030	3	0.15789		100031	3	-0.157922	
	100032	3	-0.079125		100033	3	-0.042589	
	100034	3	-0.013769		100035	3	0.01898	
	100036	3	0.06182		100037	3	0.10369	
	100038	3	0.10569		100039	3	0.0922	
	100040	3	0.15789		100041	3	-0.157922	
	100042	3	-0.079125		100043	3	-0.042589	
	100044	3	-0.013769		100045	3	0.01898	
	100046	3	0.06182		100047	3	0.10369	
	100048	3	0.10569		100049	3	0.0922	
	100050	3	0.15789		100051	3	-0.157922	
	100052	3	-0.079125		100053	3	-0.042589	
	100054	3	-0.013769		100055	3	0.01898	
	100056	3	0.06182		100057	3	0.10369	
	100058	3	0.10569		100059	3	0.0922	
	100060	3	0.15789		100061	3	-0.157922	
	100062	3	-0.079125		100063	3	-0.042589	
	100064	3	-0.013769		100065	3	0.01898	
	100066	3	0.06182		100067	3	0.10369	
	100068	3	0.10569		100069	3	0.0922	
	100070	3	0.15789		100071	3	-0.157922	
	100072	3	-0.079125		100073	3	-0.042589	
	100074	3	-0.013769		100075	3	0.01898	
	100076	3	0.06182		100077	3	0.10369	
	100078	3	0.10569		100079	3	0.0922	
	100080	3	0.15789		100081	3	-0.157922	
	100082	3	-0.079125		100083	3	-0.042589	
	100084	3	-0.013769		100085	3	0.01898	
	100086	3	0.06182		100087	3	0.10369	
	100088	3	0.10569		100089	3	0.0922	
	100090	3	0.15789		100091	3	-0.157922	
	100092	3	-0.079125		100093	3	-0.042589	
	100094	3	-0.013769		100095	3	0.01898	
	100096	3	0.06182		100097	3	0.10369	
	100098	3	0.10569		100099	3	0.0922	
	100100	3	0.15789		101001	3	-0.157922	
	101002	3	-0.079125		101003	3	-0.042589	
	101004	3	-0.013769		101005	3	0.01898	
	101006	3	0.06182		101007	3	0.10369	
	101008	3	0.10569		101009	3	0.0922	
	101010	3	0.15789		101011	3	-0.157922	

	101012	3	-0.079125		101013	3	-0.042589	
	101014	3	-0.013769		101015	3	0.01898	
	101016	3	0.06182		101017	3	0.10369	
	101018	3	0.10569		101019	3	0.0922	
	101020	3	0.15789		101021	3	-0.157922	
	101022	3	-0.079125		101023	3	-0.042589	
	101024	3	-0.013769		101025	3	0.01898	
	101026	3	0.06182		101027	3	0.10369	
	101028	3	0.10569		101029	3	0.0922	
	101030	3	0.15789		101031	3	-0.157922	
	101032	3	-0.079125		101033	3	-0.042589	
	101034	3	-0.013769		101035	3	0.01898	
	101036	3	0.06182		101037	3	0.10369	
	101038	3	0.10569		101039	3	0.0922	
	101040	3	0.15789		101041	3	-0.157922	
	101042	3	-0.079125		101043	3	-0.042589	
	101044	3	-0.013769		101045	3	0.01898	
	101046	3	0.06182		101047	3	0.10369	
	101048	3	0.10569		101049	3	0.0922	
	101050	3	0.15789		101051	3	-0.157922	
	101052	3	-0.079125		101053	3	-0.042589	
	101054	3	-0.013769		101055	3	0.01898	
	101056	3	0.06182		101057	3	0.10369	
	101058	3	0.10569		101059	3	0.0922	
	101060	3	0.15789		101061	3	-0.157922	
	101062	3	-0.079125		101063	3	-0.042589	
	101064	3	-0.013769		101065	3	0.01898	
	101066	3	0.06182		101067	3	0.10369	
	101068	3	0.10569		101069	3	0.0922	
	101070	3	0.15789		101071	3	-0.157922	
	101072	3	-0.079125		101073	3	-0.042589	
	101074	3	-0.013769		101075	3	0.01898	
	101076	3	0.06182		101077	3	0.10369	
	101078	3	0.10569		101079	3	0.0922	
	101080	3	0.15789		101081	3	-0.157922	
	101082	3	-0.079125		101083	3	-0.042589	
	101084	3	-0.013769		101085	3	0.01898	
	101086	3	0.06182		101087	3	0.10369	
	101088	3	0.10569		101089	3	0.0922	
	101090	3	0.15789		101091	3	-0.157922	
	101092	3	-0.079125		101093	3	-0.042589	
	101094	3	-0.013769		101095	3	0.01898	
	101096	3	0.06182		101097	3	0.10369	
	101098	3	0.10569		101099	3	0.0922	
	101100	3	0.15789		102001	3	-0.157922	
	102002	3	-0.079125		102003	3	-0.042589	
	102004	3	-0.013769		102005	3	0.01898	
	102006	3	0.06182		102007	3	0.10369	
	102008	3	0.10569		102009	3	0.0922	

	102010	3	0.15789		102011	3	-0.157922	
	102012	3	-0.079125		102013	3	-0.042589	
	102014	3	-0.013769		102015	3	0.01898	
	102016	3	0.06182		102017	3	0.10369	
	102018	3	0.10569		102019	3	0.0922	
	102020	3	0.15789		102021	3	-0.157922	
	102022	3	-0.079125		102023	3	-0.042589	
	102024	3	-0.013769		102025	3	0.01898	
	102026	3	0.06182		102027	3	0.10369	
	102028	3	0.10569		102029	3	0.0922	
	102030	3	0.15789		102031	3	-0.157922	
	102032	3	-0.079125		102033	3	-0.042589	
	102034	3	-0.013769		102035	3	0.01898	
	102036	3	0.06182		102037	3	0.10369	
	102038	3	0.10569		102039	3	0.0922	
	102040	3	0.15789		102041	3	-0.157922	
	102042	3	-0.079125		102043	3	-0.042589	
	102044	3	-0.013769		102045	3	0.01898	
	102046	3	0.06182		102047	3	0.10369	
	102048	3	0.10569		102049	3	0.0922	
	102050	3	0.15789		102051	3	-0.157922	
	102052	3	-0.079125		102053	3	-0.042589	
	102054	3	-0.013769		102055	3	0.01898	
	102056	3	0.06182		102057	3	0.10369	
	102058	3	0.10569		102059	3	0.0922	
	102060	3	0.15789		102061	3	-0.157922	
	102062	3	-0.079125		102063	3	-0.042589	
	102064	3	-0.013769		102065	3	0.01898	
	102066	3	0.06182		102067	3	0.10369	
	102068	3	0.10569		102069	3	0.0922	
	102070	3	0.15789		102071	3	-0.157922	
	102072	3	-0.079125		102073	3	-0.042589	
	102074	3	-0.013769		102075	3	0.01898	
	102076	3	0.06182		102077	3	0.10369	
	102078	3	0.10569		102079	3	0.0922	
	102080	3	0.15789		102081	3	-0.157922	
	102082	3	-0.079125		102083	3	-0.042589	
	102084	3	-0.013769		102085	3	0.01898	
	102086	3	0.06182		102087	3	0.10369	
	102088	3	0.10569		102089	3	0.0922	
	102090	3	0.15789		102091	3	-0.157922	
	102092	3	-0.079125		102093	3	-0.042589	
	102094	3	-0.013769		102095	3	0.01898	
	102096	3	0.06182		102097	3	0.10369	
	102098	3	0.10569		102099	3	0.0922	
	102100	3	0.15789		103001	3	-0.157922	
	103002	3	-0.079125		103003	3	-0.042589	
	103004	3	-0.013769		103005	3	0.01898	
	103006	3	0.06182		103007	3	0.10369	

	103008	3	0.10569		103009	3	0.0922	
	103010	3	0.15789		103011	3	-0.157922	
	103012	3	-0.079125		103013	3	-0.042589	
	103014	3	-0.013769		103015	3	0.01898	
	103016	3	0.06182		103017	3	0.10369	
	103018	3	0.10569		103019	3	0.0922	
	103020	3	0.15789		103021	3	-0.157922	
	103022	3	-0.079125		103023	3	-0.042589	
	103024	3	-0.013769		103025	3	0.01898	
	103026	3	0.06182		103027	3	0.10369	
	103028	3	0.10569		103029	3	0.0922	
	103030	3	0.15789		103031	3	-0.157922	
	103032	3	-0.079125		103033	3	-0.042589	
	103034	3	-0.013769		103035	3	0.01898	
	103036	3	0.06182		103037	3	0.10369	
	103038	3	0.10569		103039	3	0.0922	
	103040	3	0.15789		103041	3	-0.157922	
	103042	3	-0.079125		103043	3	-0.042589	
	103044	3	-0.013769		103045	3	0.01898	
	103046	3	0.06182		103047	3	0.10369	
	103048	3	0.10569		103049	3	0.0922	
	103050	3	0.15789		103051	3	-0.157922	
	103052	3	-0.079125		103053	3	-0.042589	
	103054	3	-0.013769		103055	3	0.01898	
	103056	3	0.06182		103057	3	0.10369	
	103058	3	0.10569		103059	3	0.0922	
	103060	3	0.15789		103061	3	-0.157922	
	103062	3	-0.079125		103063	3	-0.042589	
	103064	3	-0.013769		103065	3	0.01898	
	103066	3	0.06182		103067	3	0.10369	
	103068	3	0.10569		103069	3	0.0922	
	103070	3	0.15789		103071	3	-0.157922	
	103072	3	-0.079125		103073	3	-0.042589	
	103074	3	-0.013769		103075	3	0.01898	
	103076	3	0.06182		103077	3	0.10369	
	103078	3	0.10569		103079	3	0.0922	
	103080	3	0.15789		103081	3	-0.157922	
	103082	3	-0.079125		103083	3	-0.042589	
	103084	3	-0.013769		103085	3	0.01898	
	103086	3	0.06182		103087	3	0.10369	
	103088	3	0.10569		103089	3	0.0922	
	103090	3	0.15789		103091	3	-0.157922	
	103092	3	-0.079125		103093	3	-0.042589	
	103094	3	-0.013769		103095	3	0.01898	
	103096	3	0.06182		103097	3	0.10369	
	103098	3	0.10569		103099	3	0.0922	
	103100	3	0.15789					

Appendix B: Bulk Data Entry for Aft-Wing Twist

The entires highlighted in blue are those actually used in the MSC.Nastran code

Static Moment

MOMENT	SID	G	CID	M	N1	N2	N3
MOMENT	10	1563		1.18E+06	0	1	0

SID	Load set identification number
G	Grid point identification numbr
CID	Coordinate system identification number
M	Scale Factor
Ni	Components of the vector measured in the coordinate system defined by CID

Parametric Force for Aerodynamics

AEFORCE	MACH	SYMXZ	SYMXY	UXID	MESH	FORCE	DMIK
AEFORCE	0.6	SYMM	ASYMM	20	STRUCT	10	

MACH	Mach number for this force
SYMXZ,SYMXY	Symmetry of this force vector
UXID	Identification number of a UXVEC entry that defines the control parameter associated with this downwash vector
MESH	One of AERO or STRUCT that declares whether the force vector is defined on the aerodynamic mesh or structural grid
FORCE	The ID of a FORCE/MOMENT set that defines the vector (integer > 0 if MESH = STRUCT)
DMIK	The ID of a FORCE/MOMENT set that defines the vector (character, required if MESH = AERO)

Control Parameter State

UXVEC	ID						
	LABEL1	UX1	LABEL2	UX2	~ etc. ~		

UXVEC	20						
	AFTWIST	1					

ID	Control vector identification number referenced by AEFORCE entry
LABELi	Controller name
Uxi	Magnitude of the aerodynamic extra point degree of freedom

General Controller for use in Trim

AEPARM	ID	LABEL	UNITS				

AEPARM	10	AFTWIST	NM				

ID	Controller identification number
LABEL	Controller name
UNITS	Describes units of the controller variables

Appendix C: Additional Results

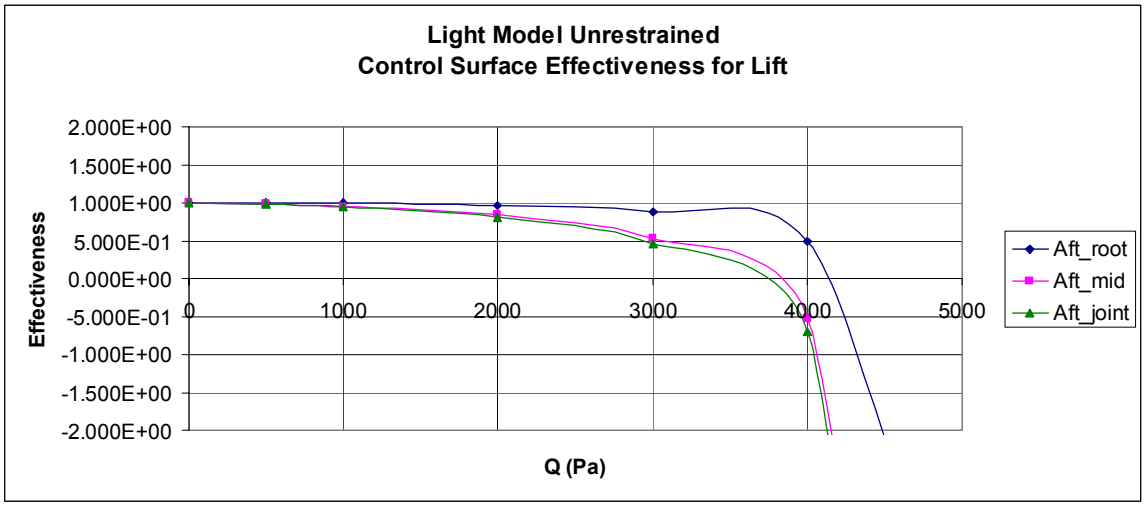

Figure C-1: Light Model Unrestrained Control Surface Effectiveness for Lift

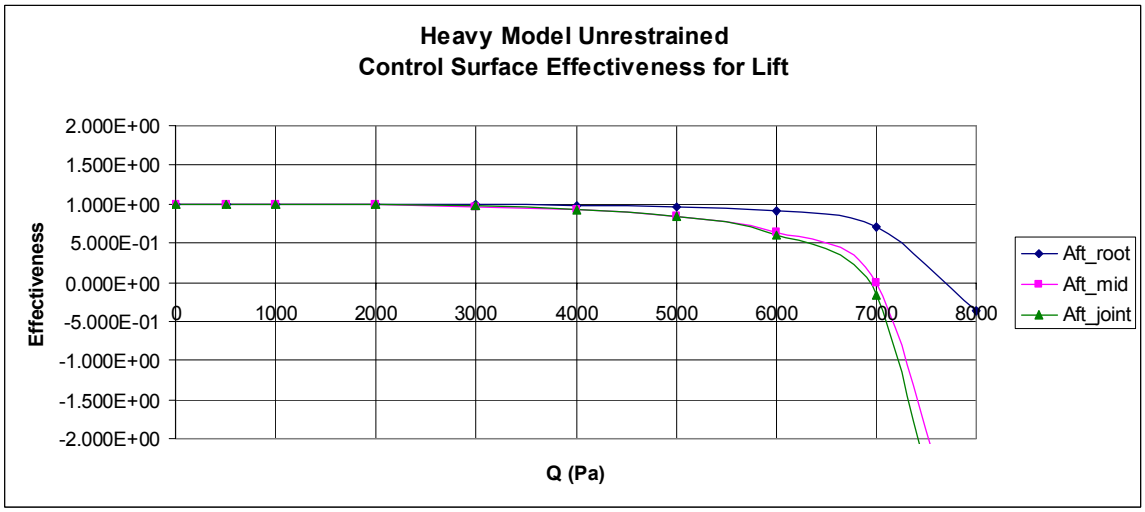

Figure C-2: Heavy Model Unrestrained Control Surface Effectiveness for Lift

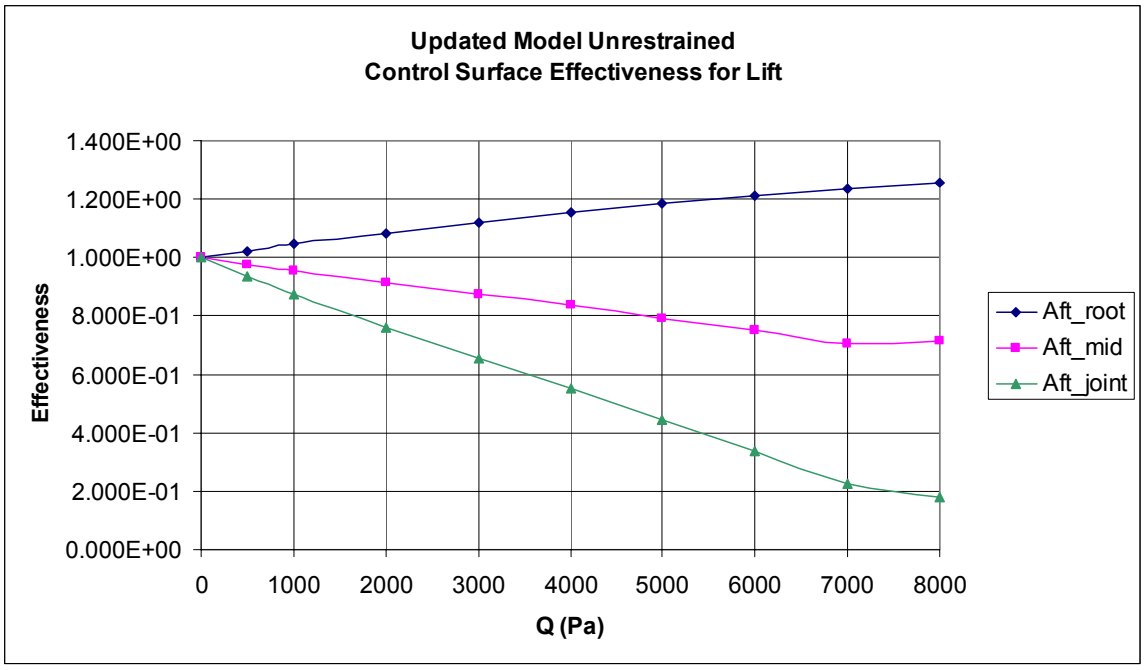

Figure C-3: Unrestrained Aft-Wing Control Surface Effectiveness at 50,000 ft

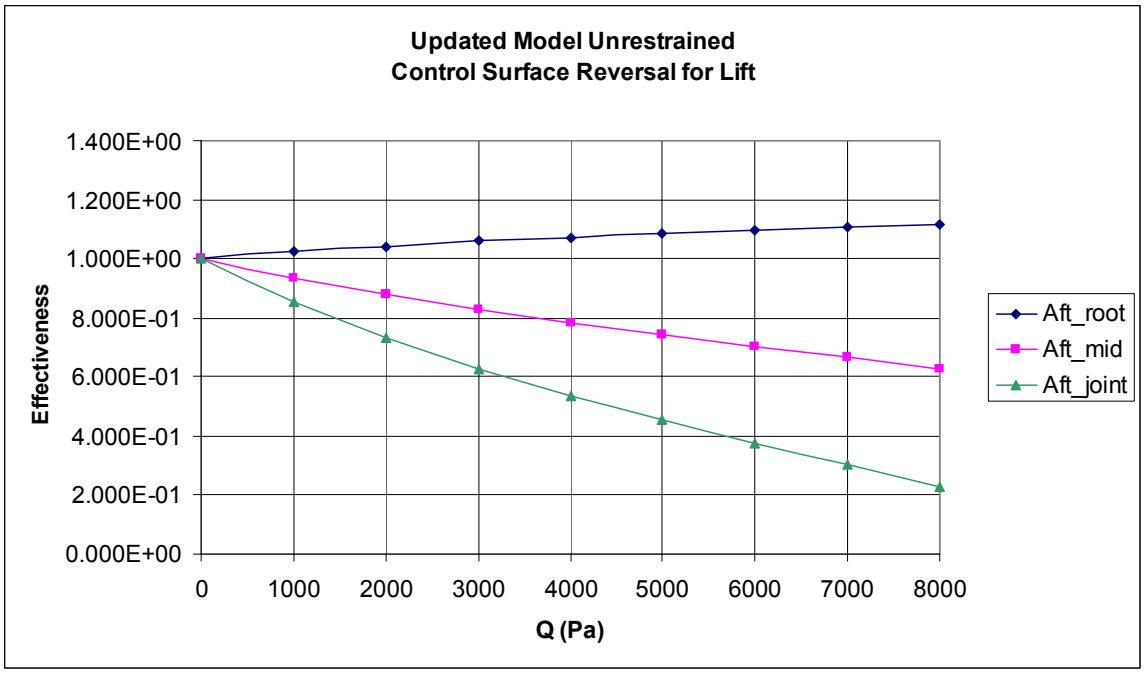

Figure C-5: Unrestrained Aft-Wing Control Surface Effectiveness at Sea Level

Bibliography

1. Roberts, Ronald. *Sensor-Craft Analytical Certification*, MS Thesis, Graduate School of Engineering, Air Force Institute of Technology (AETC), Wright-Patterson AFB, Ohio, March 2003. AFIT/GAE/ENY/03-06

2. Wolkovich, J. *Joined Wing Aircraft*, US Patent 3,942,747, March 1976.

3. Wolkovich, J. "The Joined Wing: An Overview", AIAA-1985-0274, presented at the 23rd AIAA Aerospace Sciences Meeting, Reno, NV, 14-17 January 1985.

4. Fairchild, M.P. "Structural Weight Comparison of a Joined Wing and a Conventional Wing", AIAA-81-0366, presented at the 19th AIAA Aerospace Sciences Meeting, Reno, NV, 12-15 January 1981.

5. Smith, S.C. and Cliff, S.E. "The Design of a Joined-Wing Flight Demonstrator Aircraft", AIAA-87-2930, presented at the AIAA/AHS/ASEE Aircraft Design, Systems and Operations Meeting, St. Louis, MO, 14-16 September 1987.

6. Gallman, J.W., Kroo, I.M., and Smith, S.C. "Design Synthesis and Optimization of Joined-Wing Transports", AIAA-90-3197, presented at the AIAA/AHS/ASEE Aircraft Design, Systems and Operations Meeting, Dayton, OH, 17-19 September 1990.

7. Wai, J., Herling, W.W., and Muilenburg, D.A. "Analysis of a Joined-Wing Configuration", presented at the 32nd Aerospace Sciences Meeting and Exhibit, Reno, NV, 10-13 January 1994.

8. Tyler, C., Schwabacher, G., Carter, D. "Comparison of Computational and Experimental Studies for a Joined-Wing Aircraft", AIAA-94-0657, presented at the 40th AIAA Aerospace Sciences Meeting and Exhibit, Reno, NV, 14-17 January 2002.

9. Livne, E. "Aeroelasticity of Joined-Wing Airplane Configurations: Past Work and Future Challenges – A Survey", AIAA-2001-1370, presented at the 42nd AIAA/ASME/ASCE/AHS/ASC Structures, Structural Dynamics, and Materials Conference, Seattle, WA, 16-19 April 2001.

10. Gallman, J.W. "Structural Optimization for Joined-Wing Synthesis", Journal of Aircraft, Vol. 33, No. 1, January-February 1996, pp. 214-223.

11. Reich, G.W., Raveh, D., and Zink, P.S. "Applicaton of Active Aeroelastic Wing Technology to a Joined-Wing SensorCraft", AIAA-2002-1633, presented at the 43rd AIAA/ASME/ASCE/AHS/ASC Structures, Structural Dynamics, and Materials Conference, Denver, CO, 22-25 April 2002.

12. "Adaptive Modeling Language Basic Training Manual: Version 2.07," TechnoSoft Incorporated, 2001.

13. Towne, M.C., Strande, S.M., Erickson, L.L., Kroo, I.M., Enomoto, F.Y., Carmichael, R.L., and McPherson, K.F. "PanAir Modeling Studies".

14. MSC.FlightLoads and Dynamic User's Guide, Version 2001 (r2), MSC.Software Corporation, Santa Ana, CA, 2001.

15. MSC/Nastran Aeroelastic Analysis User's Guide, V68, W. P. Rodden and E. H. Johnson, The MacNeal-Schwendler Corporation, Los Angeles, CA, 1994.

16. MSC.visualNastran Quick Reference Guide, MSC.Nastran 2001, MSC.Software Corporation, Los Angeles, CA, 2001.

17. Blair, M., Moorhouse, D., and Weisshaar, T.A. "System Design Innovation Using Multidisciplinary Optimization and Simulation", AIAA 2000-4705, presented at the 8th AIAA/USAF/NASA/ISSMO Symposium on Multidisciplinary Analysis and Optimization at Long Beach, CA, 6-8 September 2000.

18. Strang, W.Z., Tomaro, R.F., and Grismer, M.J. "The Defining Methods of *Cobalt*$_{60}$: A Parallel, Implicit, Unstructured Euler/Navier-Stokes Flow Solver", AIAA-99-0786, presented at the 37th AIAA Aerospace Sciences Meeting and Exhibit, Reno, NV, 11-14 January 1999.

19. Blair, M., and Canfield, R.A. "A Joined-Wing Structural Weight Modeling Study", AIAA-2002-1337, presented at the 43rd AIAA/ASME/ASCE/AHS/ASC Structures, Structural Dynamics and Materials Conference, Denver, CO, 22-25 April 2002

20. Roberts, R., Canfield, R.A., and Blair, M. "SensorCraft Structural Optimization and Analytical Certification," 44rth AIAA/ASME/ASCE/AHS/ASC Structures, Structural Dynamics, and Materials Conference, Norfolk, VA, 7-10 April 2003, AIAA-2003-1458.

21. Rasmussen, Cody. "Optimization Process for Configuration of a Flexible Joined-Wing", MS Thesis, Graduate School of Engineering, Air Force Institute of Technology (AETC), Wright-Patterson AFB, Ohio, March 2004. AFIT/GAE/ENY/04-M14

Vita

Lieutenant Jennifer J. Sitz grew up in Merrill, Wisconsin and graduated from Merrill Senior High. She attended Rose-Hulman Institute of Technology in Terre Haute, Indiana, where she participated in Air Force ROTC. She graduated with a Bachelor of Science in Mechanical Engineering and was commissioned in May 2000.

Her first assignment was at the Air Vehicles Directorate of the Air Force Research Library, where she was an aerodynamic design engineer for UAVs. She then worked for the Plans and Programs Directorate, first as the UAV Portfolio Manager, and is currently the Executive Officer.

REPORT DOCUMENTATION PAGE

Form Approved
OMB No. 074-0188

1. REPORT DATE *(DD-MM-YYYY)*	2. REPORT TYPE	3. DATES COVERED *(From – To)*
15-06-2004	**Master's Thesis**	5 Oct 2001 – 15 Jun 2004

4. TITLE AND SUBTITLE

AEROELASTIC ANALYSIS OF A JOINED-WING SENSORCRAFT

5a. CONTRACT NUMBER

5b. GRANT NUMBER

5c. PROGRAM ELEMENT NUMBER

6. AUTHOR(S)

Sitz, Jennifer, J., Lieutenant, USAF

5d. PROJECT NUMBER

5e. TASK NUMBER

5f. WORK UNIT NUMBER

7. PERFORMING ORGANIZATION NAMES(S) AND ADDRESS(S)

Air Force Institute of Technology
Graduate School of Engineering and Management (AFIT/EN)
2950 Hobson Way
WPAFB OH 45433-7765

8. PERFORMING ORGANIZATION REPORT NUMBER

AFIT/GAE/ENY/04-J12

9. SPONSORING/MONITORING AGENCY NAME(S) AND ADDRESS(ES)

Dayton Area Graduate Studies Institute (DAGSI)
Attn: Dr. Elizabeth Downie
3155 Research Blvd., Ste. 205
Kettering, Ohio 45420
COMM: 937-781-4000

10. SPONSOR/MONITOR'S ACRONYM(S)

11. SPONSOR/MONITOR'S REPORT NUMBER(S)

12. DISTRIBUTION/AVAILABILITY STATEMENT

APPROVED FOR PUBLIC RELEASE; DISTRIBUTION UNLIMITED.

13. SUPPLEMENTARY NOTES

14 ABSTRACT

This study performed an aeroelastic analysis of a joined-wing SensorCraft. The analysis was completed using an aluminum structural model that was splined to an aerodynamic panel model. The force and pressure distributions were examined for the four aerodynamic panels: aft wing, fore wing, joint, and outboard tip. Both distributions provide the expected results (elliptical distribution), with the exception of the fore wing. The fore wing appears to be affected by interference with the joint. The use of control surfaces for lift and roll was analyzed. Control surfaces were effective throughout most of the flight profile, but may not be usable due to radar requirements. The aft wing was examined for use in trimming the vehicle. Also, two gust conditions were examined. In one model, the wing twist was simulated using a series of scheduled control surfaces. Trim results (angle of attack and twist angle) were compared to those of previous studies, including gust conditions. The results are relatively consistent with those calculated in previous studies, with variations due to differences in the aerodynamic modeling. To examine a more physically accurate representation of aft wing twist, it was also modeled by twisting the wing at the root. The twist was then carried through the aft wing by the structure. Trim results were again compared to previous studies. While consistent for angle of attack results, the aft wing twist deflection remained relatively constant throughout the flight profile and requires further study.

15. SUBJECT TERMS

SensorCraft, Joined-Wing, Aeroelastic, Panel Method, Aerodynamic Analysis, Aft Wing Twist

16. SECURITY CLASSIFICATION OF:			17. LIMITATION OF ABSTRACT	18. NUMBER OF PAGES	19a. NAME OF RESPONSIBLE PERSON
a. REPORT	b. ABSTRACT	c. THIS PAGE			CANFIELD, ROBERT A., Lieutenant Colonel, USAF
U	U	U	UU	83	19b. TELEPHONE NUMBER *(Include area code)* DEPT PHONE – 937-255-3069, robert.canfield@afit.edu